The study on Endoplasmic Reticulum-Mitochondria relationship in Tocopheryl ester induced Apoptosis

2023

Manobendro Nath Ray

Contents

Figure Index

Abstract

The esters of α-tocopherol have drawn the attraction of researchers for their versatile biological functions. Recently, α-tocopheryl succinate (TS), a redox-silent succinyl ester of natural α-tocopherol, has emerged as a novel anticancer agent. Several reports have shown that TS inhibits mitochondrial respiratory complex II and generates superoxide and cause apoptosis. Another research suggests that endoplasmic reticulum (ER) stress was involved in TS-induced apoptosis. Furthermore, the terminal ester moiety of tocopheryl esters contributes to apoptosis induction. However, the ER-mitochondria relationship and the influence of the ester moiety of tocopheryl esters in this relationship are unclear. In this study, I found that TS increased intracellular superoxide and Ca^{2+} in cultured cells, suggesting induction of ER stress. In addition, TS downregulated glucose-regulated protein 78 (GRP78), which maintains ER homeostasis and promotes cell survival, further supporting ER stress induction. Moreover, TS caused mitochondrial depolarization. However, inositol 1,4,5-trisphosphate (IP_3) receptor antagonist 2-aminoethyl diphenylborinate (2-APB) which is the inhibitor of Ca^{2+} efflux, decreased TS-induced intracellular Ca^{2+}, restored mitochondrial activity and cell viability in TS-treated cells, establishing the ER-mitochondria relationship in apoptosis induction by TS. Further investigation on the ER-mitochondria contact site revealed that TS-treated cells exhibited increased ER-mitochondria contact compared to the control cells. These results confirm a potential relationship between ER and mitochondria in apoptosis induction. Furthermore, to investigate the role of the terminal ester moiety of the TS on this ER-mitochondria relationship, I compared the apoptogenic ability of TS, which has four carbon atoms in the terminal ester moiety, to that of a newly synthesized, tocopheryl glutarate (Tglu), which has five. Cytotoxicity assays *in vitro* confirmed that TS stimulated apoptosis, while Tglu was non-cytotoxic. In investigating biological mechanisms leading to these opposing effects, I found that Tglu treatment upregulated GRP78 but did not elevate intracellular superoxide and Ca^{2+}, and thus no mitochondrial depolarization was observed like TS treatment. Taken together, these results suggest a model in which TS-mediated superoxide production and GRP78 inhibition induce ER stress, which elevates intracellular Ca^{2+} and, at the same time, increases ER-mitochondria contact and mitochondrial depolarization, leading to apoptosis. Because Tglu does not affect superoxide generation and increases GRP78 expression, it inhibits ER stress and is thereby non-cytotoxic. Moreover, increasing the carbon number in the terminal ester moiety by only one carbon results in the opposite regulation of the ER-mitochondria relationship.

Chapter 1
Introduction

Chapter 1: Introduction

1.1 Tocopheryl esters

Vitamin E refers to a group of eight structurally related (Fig. 1.1) lipid soluble compounds: four tocopherol isomers (α-, β-, γ-, and δ-tocopherols) and four tocotrienols isomers (α-, β-, γ-, and δ-tocotrienols). Among them, the α-tocopherol is the most biologically active form (*Sies H, 1991*). The free radical capturing ability of α-tocopherol due to the presence of the hydroxyl (-OH) group makes it a potent antioxidant. In addition, α-tocopherol decreases the activity of several enzymes such as nicotinamide adenine dinucleotide phosphate (NADPH) oxidases, protein kinase C (PKC), and phospholipase A2 (*Azzi A, 2003*). However, the easily oxidizable property of α-tocopherol makes it relatively unstable.

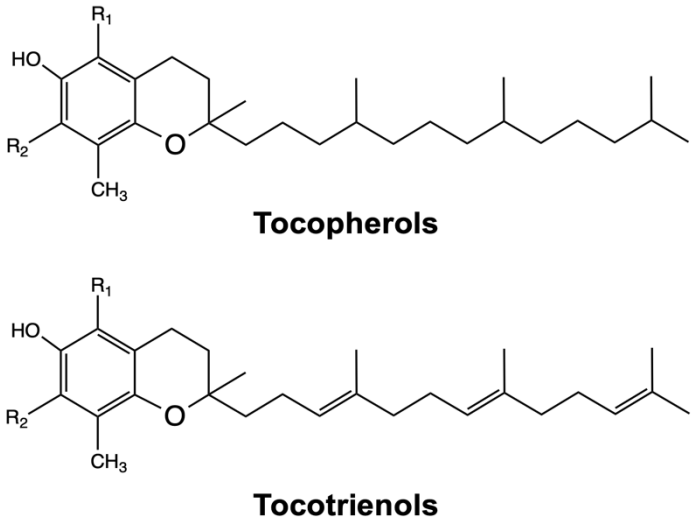

	R_1	R_2
α	CH_3	CH_3
β	H	CH_3
γ	CH_3	H
δ	H	H

Fig. 1.1: Structure of tocopherols and tocotrienols

The esterification of α-tocopherol solves this stability issue of natural α-tocopherol. Because in the esterified forms the reactive hydroxyl group (-OH) is protected from oxidation and hence have longer shelf life (*Papas AM, 1993*). In addition, several esters of tocopherols such as tocopheryl acetate, tocopheryl succinate, tocopheryl linoleate, tocopheryl nicotinate, and potassium ascorbyl tocopheryl phosphate are being used as antioxidants in different cosmetic formulations.

Recently, α-tocopheryl succinate (TS) was identified as a novel anticancer agent, potentially via its interaction with apoptotic machinery. TS is a fat-soluble succinyl ester of

naturally occurring α-tocopherol (Fig. 1.2). Multiple researchers have considered it the most effective form of vitamin E in inducing apoptosis in cancer cells (*Prasad KN, 2003*). TS induces apoptosis preferentially in the cancer cell with limited toxicity toward normal cells (*Neuzil J, 2001*). The mechanisms by which apoptosis is induced by TS are complex, and they have not yet been completely elucidated. The understanding of the cytotoxic mechanisms of TS and related tocopheryl esters may provide information about new molecular targets for killing cancer cells and thereby improving cancer therapy.

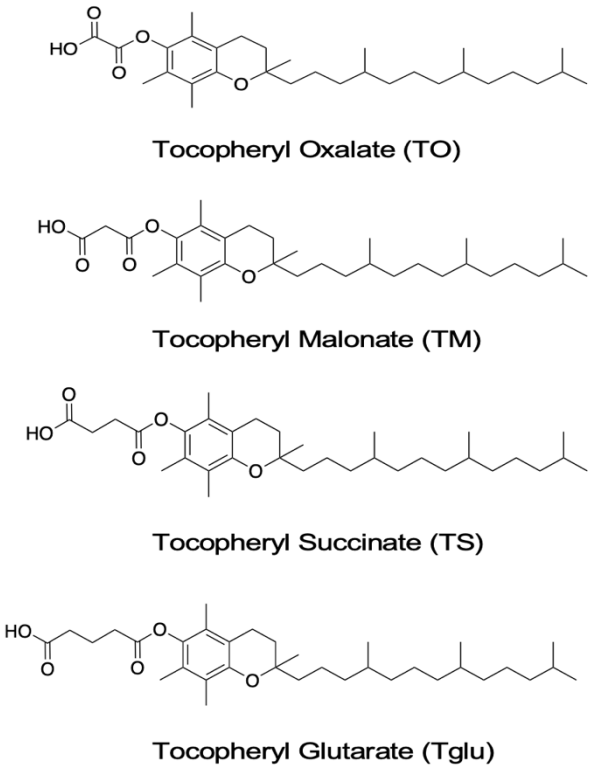

Fig.1.2: Structure of α-tocopheryl esters

1.2 Mechanism of TS induced apoptosis

TS has been shown to induce the production of reactive oxygen species (ROS) by interfering with the electron transferring activity of the mitochondrial respiratory complex I and II (*Dong LF, 2008; Dos Santos GAS, 2011; Kluckova K, 2013; Yan B, 2015*). In addition, TS inhibits mitochondrial glycerol-3-phosphate dehydrogenase, an enzyme that transfers glycolysis generated electron to the mitochondrial respiratory chain (*Rauchova H, 2014*). Thus, the interruption in the electron transfer system of the mitochondria causes leakage of electron

from the mitochondrial respiratory chain (Fig. 1.3). Afterwards, the leaked electron from the mitochondrial respiratory chain interacts with oxygen (O_2) to generate superoxide (O_2^-). The resulting oxidative stress due to the superoxide accumulation activates apoptotic pathways in various types of cancer cell (*Kogure K, 2001, Dong LF, 2008; Dos Santos, 2011; Kluckova K, 2013; Yan B, 2015*). In addition, the ROS-generating capability of TS has also been shown to correlate with endoplasmic reticulum (ER) stress and apoptosis in human gastric cancer cell (*Huang X, 2010; Huang X, 2013*).

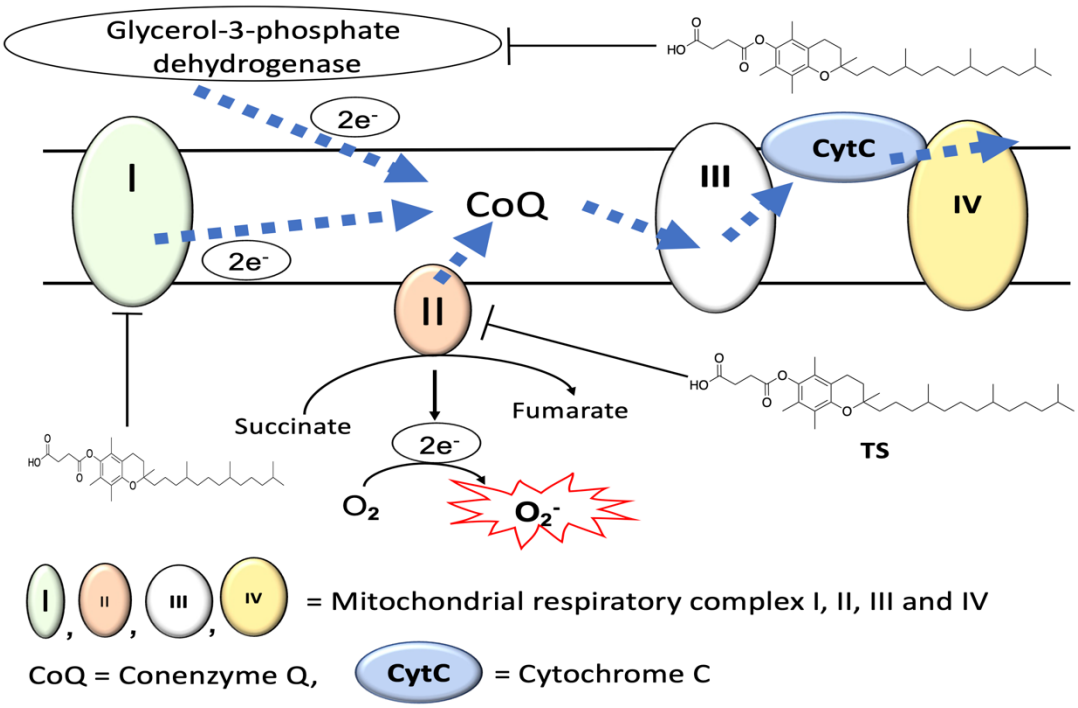

Fig. 1.3: Mechanism of superoxide generation by TS

TS interrupts the electron transport through mitochondrial respiratory chain by inhibiting mitochondrial respiratory complex-I and II, and mitochondrial glycerol-3-phosphate dehydrogenase. The leaked electron from the respiratory chain interacts with oxygen to generate superoxide.

1.3 The involvement of ER stress in apoptosis

Recently, ER stress and related apoptotic pathways have emerged as an attractive field of study for the development of effective cancer pharmacotherapies (*Fu X, 2021*). Oncogene activation, loss of tumour suppressors, hypoxia, nutrient deprivation and acidosis cause the generation of misfolded proteins in cancer cells (*Tameire F, 2015*). The protein quality control (PQC) system encompassing the chaperone system and protein degradation system controls the

number of misfolded proteins within the cells. Depending on the functionality of these two systems, the amount of misfolded protein may vary in the cancer cells. Usually, these systems are defective in the cancer cells due to gene mutation, hostile microenvironment, inflammation, and rapid ROS production. The lack of clearance of misfolded proteins due to the dysfunctional PQC of the cancer cells causes misfolded proteins accumulate within the cells. However, the type and quantity of the accumulated misfolded proteins in the cancer cells are unknown. These defective proteins subject the ER to stress, and the organelle consequently activates a highly conserved adaptive survival mechanism, the unfolded protein response (UPR), to support cancer cell survival (*Ojha R, 2017; Hsu SK, 2019*). UPR, however, fails to manage misfolded proteins and prevent apoptosis when ER stress is prolonged (*Kara M, 2020; Sano R, 2013; Szegezdi E, 2006*).

Chaperones are proteins from 70 kDa heat-shock (Hsp70s) protein family that are involved in a plethora of processes including folding of newly synthesized proteins, transportation of the proteins across the membranes, refolding of misfolded and aggregated proteins (*Bakau B, 2006*). Glucose-regulated protein (GRP78) is a key ER-resident molecular chaperone and is also known as the master regulator of UPR signal transduction. Accordingly, GRP78 has been found to be overexpressed in various cancer cells (*Ibrahim IM, 2019*). GRP78 keeps unfolded protein concentrations to a minimum and thus protects the cancer cells from UPR-mediated apoptosis (*Elfiky AA, 2020*). Several recent studies have suggested that downregulation of GRP78 inhibits the proliferation and migration of various cancer cells, enhances their radio- and chemo-sensitivity, and ultimately facilitates the killing of cancer cells by other therapeutics (*Booth L, 2012; Yun S, 2017; Kao C, 2018; Liang G, 2018; Yu X, 2018; Sharma SH, 2018*). In these regards, then, GRP78 represents a potential target for the induction of ER stress by TS, but experimental evidence to support this hypothesis is not yet available.

1.4 Role ER-Mitochondria contact in apoptosis

Inter-organelle communication, particularly the structural and functional interaction between ER and mitochondria is an emerging aspect in investigating several cellular processes or signalling pathways including cellular apoptosis (*Rieusset J, 2018*). ER and mitochondrial membrane interacts with each other and forms an interface of 10 nm which is known as mitochondria associated ER membrane (MAM). MAM serves as a complex hub for carrying out various essential cellular pathways such as lipid synthesis, calcium exchange, mitochondrial DNA replication, apoptosis, and autophagy (*Hamasaki M, 2013; Marchi S, 2014; Lewis SC, 2016; Martinvalet D, 2018; Giamogante F, 2021*). Ca^{2+} transfer from ER to

mitochondria is one of the best examples of a pathway that is critically dependent on the ER-mitochondria contact and that leads to regulation of cell survival (*Csordás G, 2010*). The inositol 1,4,5-trisphosphate receptor (IP_3R), the main ER Ca^{2+} release channel on ER, and voltage-dependent anion channel (VDAC), an outer mitochondrial membrane ion channel, exist in a complex with the chaperone glucose-regulated protein 75 kDa (GRP75) in the MAM fraction (*Szabadkai G, 2006*). However, proper assembly of these proteins in the MAMs enhances the contact between ER and mitochondria and creates a microdomain of high Ca^{2+} concentration, which is necessary to allow uptake by the low-affinity mitochondrial Ca^{2+} uniporter (MCU) (Fig. 1.4).

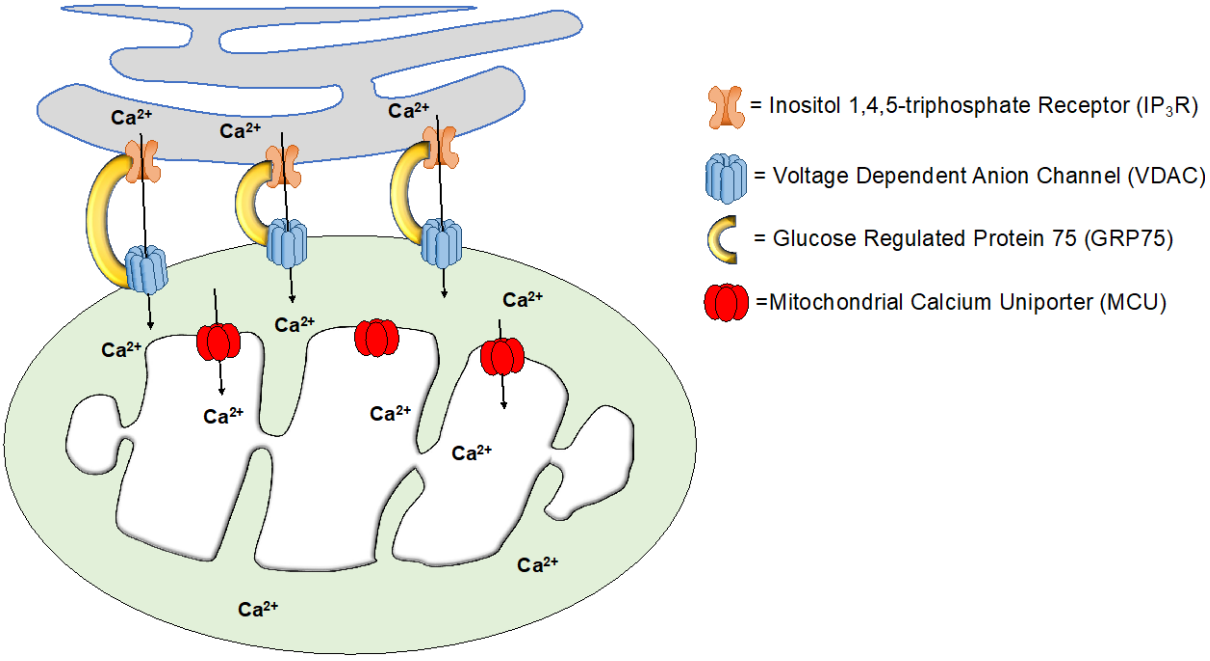

Fig. 1.4: Components of the ER-mitochondria contact site

The IP_3R channel on the ER and VDAC channel of mitochondria forms complex via GRP75 protein and creates a microdomain. Ca^{2+} flows from ER to mitochondria through this microdomain and later uptaken in the mitochondrial matrix by the MCU.

Recently, GRP75 has emerged as the major component of the MAM that plays a key role in mitochondrial homeostasis (*D'Eletto M, 2018; Zhao Q, 2021*). In addition, GRP75 mediates ER and mitochondrial coupling and causes calcium dependent apoptosis in cancer and diabetic retinopathy (*Tiwary S, 2021; Li J, 2022; Li Y, 2022*).

GRP75 is mostly located in the mitochondrial matrix, but a low level of GRP75 is found in the cytoplasm plasm and nucleus (*Wadhwa R, 2002*). Cytoplasmic GRP75 acts as a link between IP_3R and VDAC that enables close juxtaposition between ER and mitochondria to regulate Ca^{2+} transfer from ER to mitochondria. Therefore, GRP75 may be a possible target to manipulate the Ca^{2+} transfer from ER to mitochondria and thereby affecting cellular processes like apoptosis.

1.5 Structure activity relationship of the tocopheryl esters in apoptosis induction

While direct targets of α-tocopherol derivatives have not yet been identified, structure-activity relationship studies have suggested that the pro-apoptotic activity of these molecules depends on the length and charge of the terminal ester moiety (*Birringer M, 2003*). Previously, it was reported that other derivatives of α-tocopherol, α-tocopheryl oxalate and α-tocopheryl malonate (Fig. 1.2) also have pro-apoptotic activity (*Kogure K, 2005*). Interestingly, the strength of the pro-apoptotic activity differs among these derivatives, with α-tocopheryl oxalate having the highest activity among the derivatives tested. Furthermore, the terminal dicarboxylate moiety must contain four or less than four carbon atoms in order for a derivative of α-tocopherol to display pro-apoptotic activity (*Kogure K, 2004*).

1.6 Objective of the thesis

Despite the correlative understanding of the influence of structure of tocopheryl ester derivatives on their activity, the mechanisms by which the side chain length of α-Tocopherol derivatives affect pro-apoptotic activity are unknown. In addition, the relationship between ER and mitochondria in tocopheryl ester induced apoptosis is not elucidated yet. Furthermore, the effect of tocopheryl ester on MAM is unknown.

Therefore, the objective of my thesis is to investigate the relationship between ER and mitochondria in tocopheryl ester induced apoptosis, the role of terminal ester moiety in apoptosis induction and the effect of tocopheryl ester on the MAM.

Chapter 2

Investigating the mechanism of Tocopheryl ester induced apoptosis and their structure activity relationship

Chapter 2: Investigating the mechanism of Tocopheryl ester induced apoptosis and their structure activity relationship

2.1 Introduction

I hypothesized that the conformational flexibility of tocopheryl ester derivatives or their ability to interact with molecular targets results in variation in some biological activities of different α-tocopheryl esters, including intracellular superoxide production and ER stress induction.

To test my hypothesis, in this chapter I have compared the pro-apoptotic activities of TS and a newly synthesized tocopheryl ester, α-tocopheryl glutarate (Tglu). These molecules are identical chemically, except that TS contains four carbon atoms in the terminal ester moiety, while Tglu contains five (Fig. 1.2). By examining the individual effects of TS and Tglu on intracellular superoxide production, ER stress, mitochondrial integrity, and apoptosis *in vitro*, I was able to gain insight into structural requirements for the cytotoxic biological activities of α-tocopherol derivatives.

2.2 Materials and Methods

2.2.1 Materials

TS and egg phosphatidylcholine were purchased from Sigma-Aldrich (St. Louis, MO, USA). Glutaric anhydride, 4-dimethylaminopyridine, and D-α-tocopherol were purchased from Tokyo Chemical Industry (Tokyo, Japan). Tetrahydrofuran was purchased from Kanto Chemical (Tokyo, Japan). Other reagents were of the highest grade commercially available.

2.2.2 Synthesis of α-tocopheryl glutarate

Tglu was synthesized by the condensation of D-α-tocopherol and glutaric anhydride in the presence of a catalytic amount of 4-dimethylaminopyridine. To a solution of D-α-tocopherol (201 mg, 0.467 mmol) in tetrahydrofuran (3 mL) were added glutaric anhydride (160 mg, 1.40 mmol) and 4-dimethylaminopyridine (5.7 mg, 0.0467 mmol) at room temperature. After stirring for 40 h, saturated NH_4Cl (10 mL) was added, and the mixture was then extracted twice with 20 mL of ethanol ethylacetate (AcOEt). The organic layer was washed twice with brine (15 mL), dried over anhydrous $MgSO_4$, filtered, and concentrated *in vacuo*. The residue was purified by two-column chromatography steps using an Isolara™ automated purification system (Biotage, Sweden). The first step employed a linear gradient of *n*-hexane: AcOEt from 95:5 to 70:30, and the second step employed a linear gradient of *n*-hexane: AcOEt from 10:1 to 70:30 to afford Tglu 66.4 mg (Yield = 26%) as white solid. Tglu was identified using nuclear magnetic resonance (NMR).

2.2.3 Liposome preparation

A chloroform solution (0.1 mL) containing 0.1 M TS or Tglu was mixed with 0.64 mL of a chloroform solution containing egg phosphatidylcholine (0.1 g/mL) in a glass tube. The mixture was evaporated to dryness under a nitrogen stream to form a lipid film. The lipid film was hydrated with 192 μL PBS and 8 μL 1 N NaOH. The hydrated lipid film was incubated at 55 °C for 10 min in a water bath. After the incubation, the glass test tube was sonicated in an ultrasonic bath for 10 to 15 minutes to form liposomes. The size and surface charge of the liposomes was measured with a Zetasizer Nano (Malvern Panalytical Ltd., UK).

2.2.4 Cell culture

Mouse melanoma B16F1 cells, human hepatic carcinoma HepG2 cells, and mouse 3T3-Swiss albino cells were purchased from American Type Culture Collection and were cultured in Dulbecco's modified Eagle medium (DMEM) containing 10% fetal bovine serum (FBS) and 1% penicillin-streptomycin at 37 °C in a 5% CO_2 humidified environment. When the cells reached 80% confluency, they were treated with TS or Tglu for 12 h, 24 h and 48 h time intervals.

2.2.5 Cell viability assay

Cells were seeded at a density of 1.5×10^5 cells/well in vacuum gas plasma treated 6-well plates and were cultured for 24 h. The cells were treated with different amounts of TS and Tglu-containing liposomes and incubated for 24 h and 48 h at 37 °C. The cells were collected by trypsin treatment, and cell viability was measured with the trypan blue dye exclusion method. Cell viability was calculated as the percentage of stained cells relative to the total number of cells.

2.2.6 Apoptosis analysis via DAPI staining

Cells were seeded at a density of 1.5×10^5 cells/well in a 35mm glass-bottom dish. The cells were treated with 75 µM and 100 µM TS-containing liposomes and incubated for 24 h. After 24 h, cells were fixed with 4% formaldehyde-phosphate buffer saline (PBS) at 37 °C for 15 min. Then, cells were washed with PBS and permeabilized with 0.1% Triton-bovine serum albumin (BSA) at 37 °C for 15 min. Afterwards, 1 ml DAPI (1 µg/ ml) was added to the dish and incubated the cells for another 15 min at 37 °C. After 15 min of incubation, cells were washed with PBS 3 times and observed under LSM700 confocal laser scanning microscope.

2.2.7 Corrected total cell fluorescence (CTCF) calculation

Region of interest (ROI) was drawn around a certain number of cells using polygon selection and measured the area, mean and integrated density by ImageJ. I also measured the area and mean fluorescence of the background by selecting a non-fluorescence area of the image. After that, I calculated the corrected total cell fluorescence (CTCF) using the following formula-

CTCF = Integrated Density – (Area of selected cells X Mean fluorescence of background)

2.2.8 Analysis of cytochrome c release

Mitochondria were stained using MitoTracker Deep Red FM (Cell Signaling Technology, Massachusetts, USA). Mitochondria possess a membrane potential (around -150 mV), an indicator of mitochondrial activity. On the other hand, MitoTracker dyes are cell-permeable positively charged probes that contain a mildly thiol-reactive chloromethyl moiety. When cells are incubated with MitoTracker, these probes passively diffuse across the plasma membrane and accumulate in mitochondria in a membrane potential-dependent manner. After entering mitochondria, MitoTracker probes bind to the thiol group of mitochondrial proteins and show fluorescence under the confocal microscope. After treatment with TS for 12 h, cells were washed with PBS and loaded with 500 nM MitoTracker Deep Red FM that was diluted in culture media and incubated for 30 min at 37 °C. After incubation, cells were fixed in ice-cold 100% methanol for 15 min at -20 °C. Cells were washed with PBS and permeabilized with 0.1% Triton-BSA at 37 °C for 15 min. Afterwards, cells were washed with 5% BSA-PBS three times and incubated in anti-cytochrome c antibody (ab90529; Abcam) at a dilution of 1:1000 for 1 h at 37 °C. Next, cells were washed with 5% BSA-PBS three times and incubated the cells another 1 h at 37 °C with Alexa Fluor 488-conjugated secondary antibody (secondary, dilution 1:500). Then, cells were rinsed with PBS three times and observed with an LSM700 confocal laser scanning microscope. Images were processed for background subtraction with a rolling ball radius of 50 pixels (default). Afterwards, images were converted to 16-bit images and ROI was drawn around the boundaries of 4-5 cells/image. Next, cytofluorograms and colocalization ratio (Pearson coefficient) of MitoTracker and cytochrome c were obtained using the “colocalization finder” function of the ImageJ. At least, 30 images were analyzed during each observation.

2.2.9 TMRE assay for mitochondrial membrane potential

Tetramethylrhodamine, ethyl ester (TMRE, ab113852; Abcam) is a cell-permeant, positively charged mitochondria-specific fluorescence dye that diffuses through the plasma membrane of the cells and accumulates in active mitochondria due to the relative negative charge of mitochondria. Depolarized mitochondria fail to sequester TMRE and show weak fluorescence under a confocal laser scanning microscope. After treatment, TMRE solution was added directly to the cell culture dishes to a final concentration of 200 nM and incubated the cells for 30 min at 37 °C. Next, cells were washed with PBS three times and observed under LSM700 confocal laser scanning microscope. 6-15 cells were analyzed in each image for

quantification of fluorescence intensity and corrected total cell fluorescence (CTCF) was calculated. At least 30 images were analyzed during each observation.

2.2.10 Analysis of TS and Tglu amount

I quantified the amount of TS and Tglu transferred to the cells and remained in the cell culture medium by high performance liquid chromatography (HPLC). I collected the culture medium and cells after different incubation periods, and lipids were extracted using the Folch method [61]. Briefly, cells were resuspended in 250 µl water, and 1.25 ml of chloroform/methanol (2:1) was added. The following vortex for 1 min cells was incubated on ice for 5 min and again vortexed for 1 min. The organic and aqueous phases were separated by centrifugation at 13400 g for 10 min at 4°C. The organic phase was dried under N_2 and dissolved in methanol. The extracted samples were subjected to HPLC using a column of TSKgel ODS-80T_M (150 X 4.6 mm, Tosoh Bioscience, Tokyo) and monitored TS samples at λ_{max} 286 nm, while Tglu at λ_{max} 284 nm. The solvent system used was methanol/water (99:1) for TS and methanol/water (90:10) for Tglu.

2.2.11 Superoxide detection

Cells were seeded at densities of 1.5×10^5 cells per 35mm glass-bottom dish. Intracellular superoxide anion was detected using the ROS-ID Superoxide Detection Kit (Enzo Life Sci., New York, USA) according to the manufacturer's instructions. At 60% confluency, some cells were treated with 75 µM liposome containing TS or Tglu. Other cells were pretreated with or 50 µM α-tocopherol or 5 mM NAC for 30 min prior to the addition of TS. After incubation for 3 h, the media was removed, and the cells were washed with PBS. Next, the cells were loaded with 1 mL superoxide staining solution and incubated for 30 min at 37 °C, and pyocyanin solution was added to a final concentration of 200 µM only to the culture dish representing the positive control. The cells were incubated for an additional 30 min. The cells were washed twice with wash buffer and observed with an LSM700 confocal laser scanning microscope (Carl Zeiss, Germany). To quantify fluorescence intensity, 10-30 cells were analyzed in each image and corrected total cell fluorescence (CTCF) was calculated based on the method described above.

2.2.12 Cytoplasmic Ca^{2+} detection

Cells were seeded at densities of 1.5×10^5 cells per 35mm glass-bottom dish. Some cells were treated with 75 μM liposomes containing TS or Tglu or 2-APB (Selleck Chemicals LLC, Houston, USA) for 48 h. Other cells were pre-treated with 50 μM 2-APB for 1 h, then TS-containing liposomes were added to the cells. After 48 h cells were washed with PBS and intracellular Ca^{2+} was detected using the Fluo 4 Calcium Assay Kit (Dojindo, Kumamoto, Japan) according to the manufacturer's instructions. Briefly, cells were loaded with 1 mL Fluo 4-AM reagent containing 0.04% Pluronic F-127 and 1.25 mmol/L probenecid and incubated for 1 h at 37 °C. After incubation, cells were observed with an LSM700 confocal laser scanning microscope. 6-15 cells were analyzed in each image for quantification of fluorescence intensity and corrected total cell fluorescence (CTCF) was calculated.

2.2.13 Real-time PCR

Total RNA was extracted and purified from cells with RNeasy Plus Mini kit (QIAGEN) according to the manufacturer's instructions. The total RNA concentration was determined with a Nanodrop 8000 spectrometer (Thermo Fisher Scientific). Then, cDNA was synthesized from 200 ng of total RNA with PrimeScript RT Master Mix (Perfect Real Time, Takara Bio, Otsu, Japan) using an MJ Mini Personal Thermal Cycler (Bio-Rad, Hercules, CA, USA). The reverse transcription reaction was performed at 37 °C for 15 min and 85 °C for 5 s. Real-time PCR analysis was performed using TB Green™ Premix Ex Taq™ II (Tli RNaseH Plus, Takara Bio) and a Thermal Cycler Dice Real-Time System III (Takara Bio). To analyze the mRNA levels of GRP78 and GAPDH or β actin, the cDNA was denatured at 95 °C for 30 s, followed by 40 cycles of 95 °C for 5 s and 60 °C for 30 s for amplification. The sequences of the primers used for the real-time PCR are shown in Table 1. The mRNA level of GRP78 was calculated using the $2^{-\Delta\Delta Ct}$ method by normalization relative to GAPDH or β actin.

Table 1. Sequences of primers used for real-time PCR

Primer	Sequence (5' to 3')
Mouse GRP78 forward	AGAAACTCCGGCGTGAGGTAGA
Mouse GRP78 reverse	TTCCTGGACAGGCTTCATGGTAG
Mouse GAPDH forward	GAGGACCAGGTTGTCTCCTG
Mouse GAPDH reverse	ATGTAGGCCATGAGGTCCAC
Human GRP78 forward	TGGGTCGACTCGAATTCCAAAG
Human GRP78 reverse	GTCAGGCGATTCTGGTCATTGG
Human β-actin forward	CACTCTTCCAGCCTTCCTTCC
Human β-actin reverse	CGTACAGGTCTTTGCGGATGTC

2.2.14 Western blotting

The following antibodies were used: anti-GRP78 rabbit polyclonal antibody (ab21685; Abcam, Cambridge, UK), anti-GAPDH rabbit monoclonal antibody (Cell Signaling Technology, Danvers, MA, U.S.A), anti-β actin rabbit polyclonal (ab8227, Abcam), and anti-horseradish peroxidase (HRP)-conjugated goat anti-rabbit IgG polyclonal antibody (A24531; Thermo Fisher Scientific, Waltham, MA, USA). To observe the expression of GRP78 in TS-, Tglu- and α-Tocopherol treated cells, total protein (7 μg) was separated with 10% SDS-PAGE, and the proteins were electrophoretically transferred to a polyvinylidene difluoride membrane (Bio-Rad, Hercules, CA, USA). The membrane was incubated with 5% skim milk dissolved in Tris-buffered saline (pH 7.4) containing 0.1% Tween 20 for 1h at 37 °C, then with anti-GRP78 antibody (1:3000) for 24 h at 4 °C. The membrane was washed and incubated with the HRP-conjugated secondary antibody at a dilution of 1:4000 for 1 h at 37 °C. After incubation of the membrane with a chemiluminescent substrate reagent (ECL Prime; GE Healthcare, Little Chalfont, UK), bands were detected with an LAS-4000 mini system (Fuji Film, Tokyo, Japan). After GRP78 was detected, the membrane was washed three times for 45 minutes with Tri-buffered saline (pH 7.4) containing 0.1% Tween 20, incubated with an anti-GAPDH antibody (1:3000) for 24 h at 4 °C, and developed as above. Band intensities were quantified using ImageJ.

2.2.15 Immunostaining for GRP78 localization

After treatment with TS- and Tglu-containing liposomes, cells were washed twice with 0.5 mL PBS. Then, cells were fixed with 4% paraformaldehyde in PBS for 15 min at 37 °C. Following three washes with PBS containing 1% bovine serum albumin (BSA), cells were permeabilized for 15 min at 37 °C with a PBS solution containing 1% BSA and 0.1% Triton X-100. The cells were washed and incubated with the primary antibody (anti-GRP78 BiP) for 1 h at 37 °C. Following several washes, goat anti-rabbit IgG labeled with Alexa Fluor 488 (ab150077, Abcam) in 1%BSA/PBS (1:500) was added, and the cells were incubated for 1 h at 37 °C. After incubation, the cells were washed three times with 1% BSA-PBS and incubated with primary antibody (anti-calreticulin, ab92516, Abcam) for 1 h at 37 °C. Following several washes with 1% BSA-PBS, goat anti-rabbit IgG labeled with Alexa Fluor 647 (ab150079, Abcam) in 1%BSA/PBS (1:500) was added, and the cells were incubated for another 1 h at 37 °C. Afterwards, cells were rewashed, and nuclei were counterstained for 15 min with DAPI solution (1 μg/mL). The cells were washed with PBS and observed with an LSM700 confocal laser scanning microscope. I performed quantitative analysis by drawing the ROI around boundaries of 4-5 cells/image and measuring the area of the yellow signal area by the "color threshold" function of the ImageJ. Then I measured the total green signal area obtained from the green channel in the same cells. An equal number of cells was selected during the analysis of different images. At least 30 images were analyzed during each observation. The ratio was calculated by dividing the yellow signal area by the total green signal area. The ratio represents the percentage of total GRP78 located in the ER lumen.

2.2.16 Statistical analysis

Statistical significance was determined using one-way ANOVA to compare multiple groups, followed by Tukey's honestly significant difference test using JASP software. The unpaired Student's t-test was performed to calculate statistical significance between the two groups. *P* values less than 0.05 were considered to indicate statistical significance.

2.3 Results

2.3.1 Cytotoxic effects of TS and Tglu *in vitro*

To investigate the cytotoxic effects of TS and Tglu in mouse melanoma B16F1, human hepatic carcinoma HepG2 cells, and mouse 3T3-Swiss albino, I incubated the cells with different concentrations of TS and Tglu liposome for 24 and 48 h. TS was found to decrease cell viability, as measured by trypan blue exclusion assays, in all the cell lines in a dose- and time-dependent manner (Fig. 2.1A, 2.1B and 2.1C). Even a relatively low concentration (50 μM) of TS decreased cell viability to around 75% in B16F1 cells, 77% in HepG2 cells and around 91% in mouse 3T3-Swiss albino cells after 48 h. As the dose increased to 75 μM and 100 μM, the viability of B16F1 cells at 48 h decreased further, to around 68% and 65%, respectively. In addition, TS decreased the viability of HepG2 cells by around 65% and 56% at 75 μM and 100 μM concentrations, respectively. On the other hand, 75 μM and 100 μM TS treatment decreased cell viability by about 83% and 77%, respectively, in mouse 3T3-Swiss albino cells after 48 h. 75 μM and 100 μM TS treatment for 24 h also caused the formation of apoptotic bodies when we stained the nucleus of the TS-treated B16F1 cells with 4′,6-diamidino-2-phenylindole (DAPI) after 24 h of TS treatment (Fig. 2.1D). Interestingly, Tglu treatment did not show cytotoxicity in both cancer cells, even at a higher dose of 125 μM (Fig. 2.1E, 2.1F).

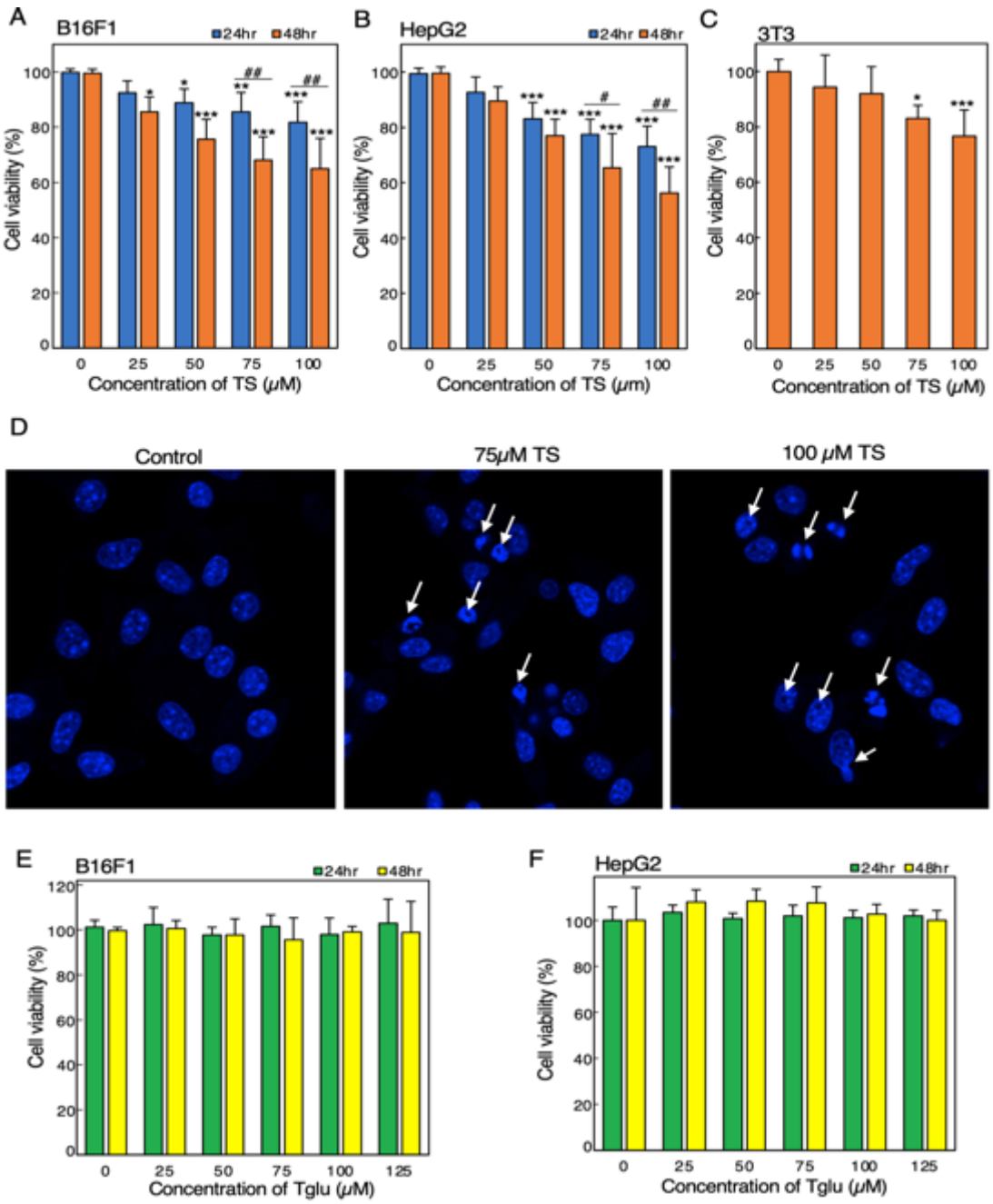

Fig. 2.1 Cytotoxicity of TS and Tglu

(A) Viability of B16F1 cells after TS treatment. (B) Viability of HepG2 cells after TS treatment. (C) Viability of mouse 3T3-Swiss albino cells after TS treatment (D) DAPI staining assay showing apoptotic bodies (arrowheads) (E) Viability of B16F1 cells after Tglu treatment. (F) Viability of HepG2 cells after Tglu treatment. Data are shown as mean ± SD (n = 6). * $P < 0.05$, ** $P < 0.01$, *** $P < 0.001$ relative to control (one way ANOVA; Tukey's Post hoc test); # $P < 0.05$, ## $P < 0.01$(unpaired Student's t-test). Scale bar = 20 µm.

2.3.2 Effect of TS on mitochondrial integrity

Mitochondrial cytochrome c release due to rupture of the outer mitochondrial membrane is the early stage of apoptosis (*Ott M, 2002*). To identify the effect of TS on mitochondrial integrity, considering cytochrome c release in the cytoplasm as an indicator, I treated the cells with 75 μM TS containing liposomes for 12 h and stained the cells with a mitochondria-specific fluorescent dye, MitoTracker and fluorescent tag antibody (secondary) that binds with cytochrome c antibody (primary). The yellow fluorescent in merged images (Fig. 2.2A) represents the localization of cytochrome c in the mitochondria. As shown in Fig. 3A, the yellow fluorescence is higher in control cells, while notable lower yellow fluorescence was observed in TS-treated cells. The cytofluorograms (Fig. 2.2B, C) obtained by the 'colocalization finder' function of ImageJ represents the correlation between the fluorescence of MitoTracker and cytochrome c. The value of the Pearson coefficient obtained from control was 0.99 and 0.45 in TS-treated cells.

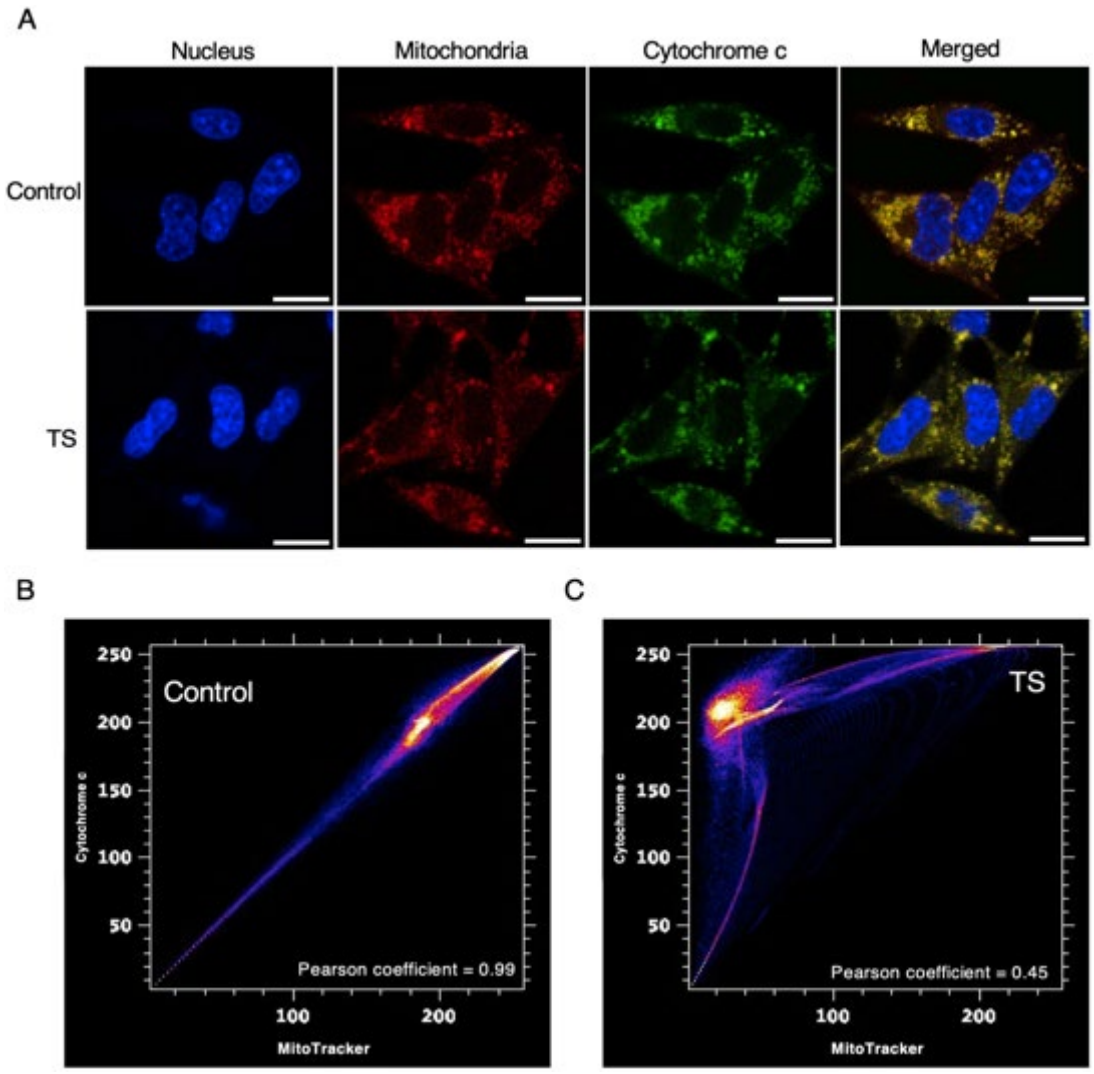

Fig. 2.2 Detection of cytochrome c release upon TS treatment

B16F1 cells were treated with 75 μM TS-containing liposomes for 12 h. Cells were incubated with MitoTracker for 30 min. After that, cells were fixed and permeabilized prior to immunostaining with an anti-cytochrome c antibody and an Alexa Fluor 647-conjugated secondary antibody. Nuclei were counterstained with DAPI (blue). Cytofluorograms were obtained using the "colocalization finder" function of ImageJ. (A) Mitochondria (Red) and cytochrome c (Green) were detected. The yellow signal in the merged images represents the localization of cytochrome c in the mitochondria. (B) Cytofluorogram of the control cells. (C) Cytofluorogram of the TS-treated cells. Individual experiments were repeated five times. Scale bar = 20 μm.

2.3.3 Effects of TS and Tglu on mitochondrial membrane potential

Mitochondrial membrane potential is a well-known indicator of mitochondrial functionality. To identify the influence of structural changes of tocopheryl esters and the involvement of the tocopheryl ester-induced altered intracellular calcium level on mitochondrial membrane potential, I treated B16F1 and HepG2 cells with TS, Tglu or 2-APB or both with TS and 2-APB for 48 h and stained the cells with tetramethylrhodamine ethyl ester (TMRE), a mitochondria-specific fluorescent dye, which accumulates in mitochondria in a membrane potential-dependent manner (Fig. 2.3). Therefore, I have considered the loss of TMRE fluorescence as a readout for mitochondrial depolarization.

TS treatment was found to correlate with decreased mitochondrial fluorescence, while Tglu and 2-APB treatment led to increased fluorescence in both cells. The quantification of fluorescence intensity by image analysis revealed that TS treatment resulted in a decrease of mitochondrial fluorescence to around 38% relative to control (Fig. 2.3C) in the B16F1 cells. In the case of HepG2 cells, TS treatment reduced mitochondrial fluorescence to around 53% relative to control. Conversely, mitochondrial fluorescence increased to around 152% and 169% of control in Tglu-treated B16F1 and HepG2 cells, respectively (Fig 2.3C, D). In addition, the IP_3R antagonist, 2-APB treated cells exhibited increased mitochondrial fluorescence of about 134% and 115% that of control in B16F1 and HepG2 cells, respectively. Notably, in the case of cells treated with both 2-APB and TS, mitochondrial fluorescence was around 89% in B16F1cells and 84% in the HepG2 cells relative to control.

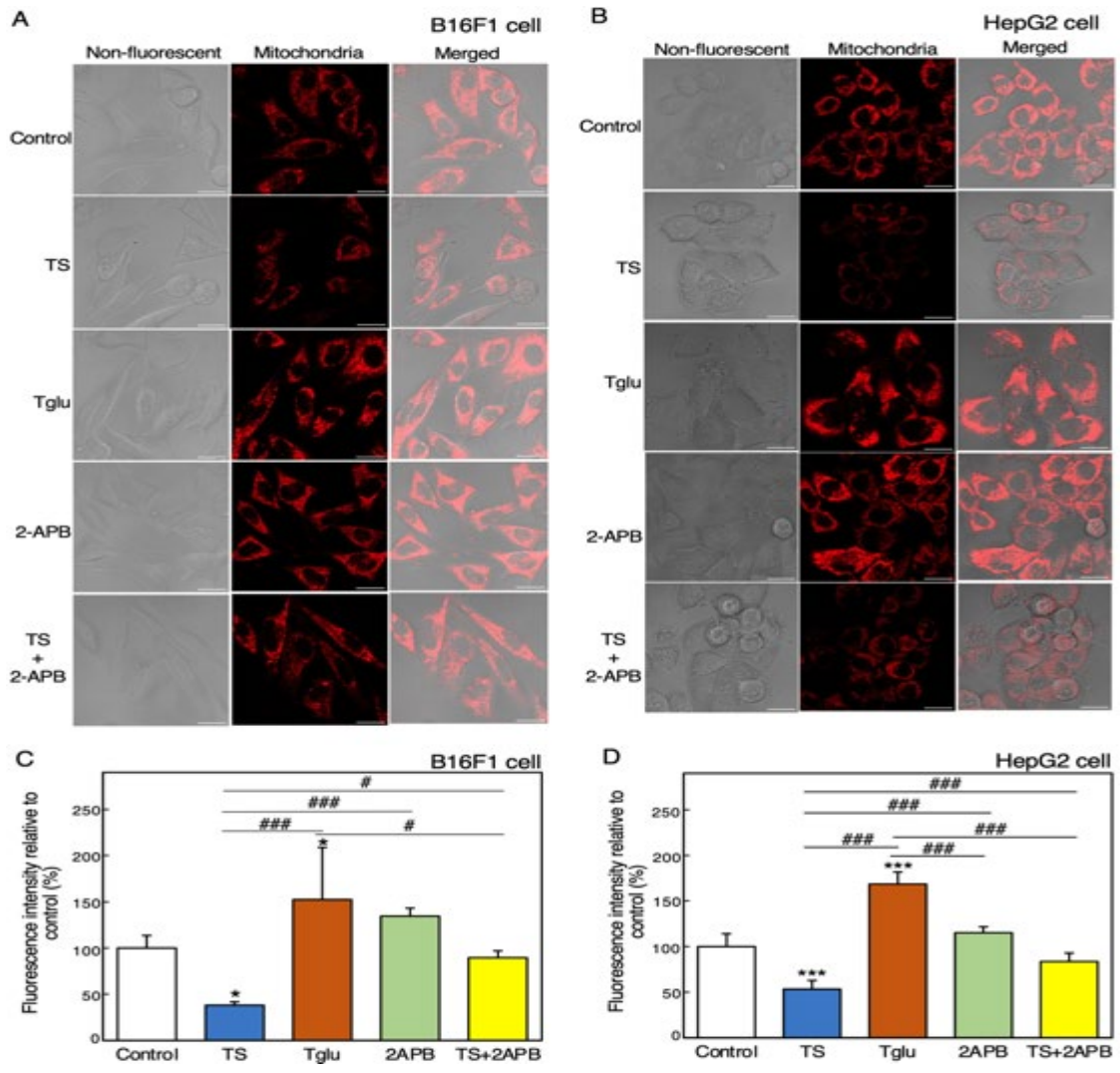

Fig. 2.3 Effects of TS and Tglu on mitochondrial membrane potential

B16F1 and HepG2 cells were treated with 75 μM TS- or Tglu-containing liposomes and inositol 1,4,5-triphosphate receptor (IP_3R) antagonist 2-aminoethyl diphenyl borinate (2-APB). Cells were pre-treated for 1 h with 50 μM 2-APB prior to the addition of TS. Mitochondria were stained with Tetramethylrhodamine, ethyl ester (TMRE). Mitochondria are stained red under confocal microscopy 48 h after treatment in B16F1 cells (A) and HepG2 cells (B). The fluorescence intensities were quantified with ImageJ (C) Quantification of fluorescence intensity in B16F1 cells. (D) Quantification of fluorescence intensity in HepG2 cells. Data are shown as mean ± SD (n = 5). * $P < 0.05$, *** $P < 0.001$ relative to control; # $P < 0.05$, ### $P < 0.001$(one way ANOVA; Tukey's Post hoc test). Scale bar = 20 μm.

2.3.4 Measurement of the amount of TS and Tglu transferred to the cell

To confirm the transfer of TS and Tglu to the cell, I quantified the amounts of TS and Tglu transferred to the cells and remaining in the culture medium by HPLC. I found that amount of TS increased intracellularly while decreasing in the cell culture medium in a time-dependent manner. Figure 2.4A shows that around 20% of the applied TS transferred to the cell immediately after adding TS to the cell culture medium. After 24 h and 48 h of addition of TS, no TS remained in the cell culture medium. However, the amount of TS found in the cells after 24 h, and 48 h was 90% and 95% of the applied TS, respectively.

In the case of Tglu, I found around 80% of applied Tglu in the cell culture medium and 20% of Tglu inside the cell immediately after adding Tglu to the cell culture medium (Fig. 2.4B). After 24 h of Tglu-addition, around 23% of applied Tglu was transferred to the cell, while about 20% of Tglu recovered from the cell culture medium. However, around 22% Tglu was found inside the cell, while no Tglu remained in the medium after 48 h.

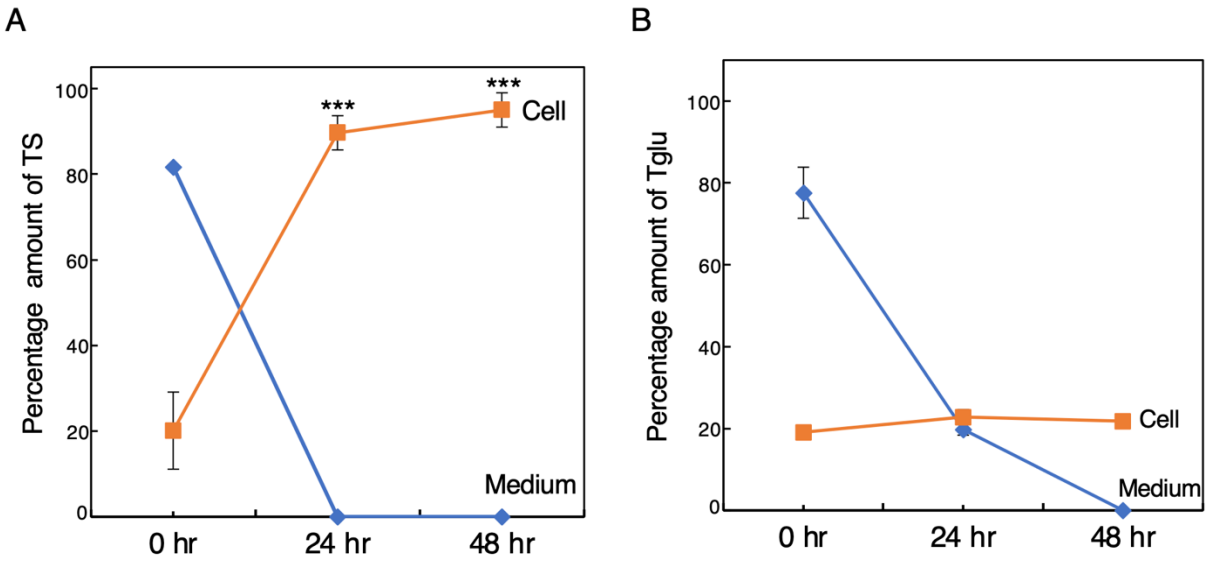

Fig. 2.4 Measurement of TS and Tglu inside the cell

B16F1 cells were separately treated with 75 μM TS- and Tglu-containing liposomes in serum-free medium. Cells and culture medium was collected after 0 h, 24 h and 48 h. The amount of TS and Tglu in the collected samples was quantified by HPLC. Data are shown as mean ± SD (n = 6). *** $P < 0.001$vs 0 h (one way ANOVA; Tukey's Post hoc test).

2.3.5 Effects of TS and Tglu on intracellular superoxide production

The induction of superoxide production is a key mechanism leading to the cytotoxicity of TS (*Kogure K, 2001; Kogure K, 2002; Dong LF, 2008*). To investigate how length of the ester moiety of the tocopheryl esters influence intracellular superoxide production, I examined the production of superoxide by B16F1 and HepG2 cells in the presence of TS and Tglu. The known superoxide-inducing bacterial metabolite pyocyanin was used as a positive control. α-Tocopherol and NAC were used as antioxidants. Superoxide was detected with a superoxide-activated fluorophore. As shown in Fig. 2.5A and 2.5C, the fluorescence intensity was notably higher in cells treated with pyocyanin or TS than in untreated cells. On the other hand, cells treated with Tglu exhibited fluorescence that was similar to that exhibited by untreated cells. According to the quantification of fluorescence by image analysis (Fig. 2.5B), pyocyanin increased intracellular superoxide production in B16F1 cells by around 186%, and TS increased intracellular superoxide by around 165%, as compared to untreated cells. On the other hand, in HepG2 cells, pyocyanin increased intracellular superoxide by around 383%, while TS increased intracellular superoxide by around 273% (Fig. 2.5D). Conversely, Tglu-treated cells exhibited similar superoxide production as did untreated cells. Notably, cells treated with both TS and α-Tocopherol exhibited around 109% and 95% of the superoxide production of untreated cells in B16F1 and HepG2 cells, respectively. NAC treatment showed about 115% superoxide production in both TS-treated B16F1 and HepG2 cells.

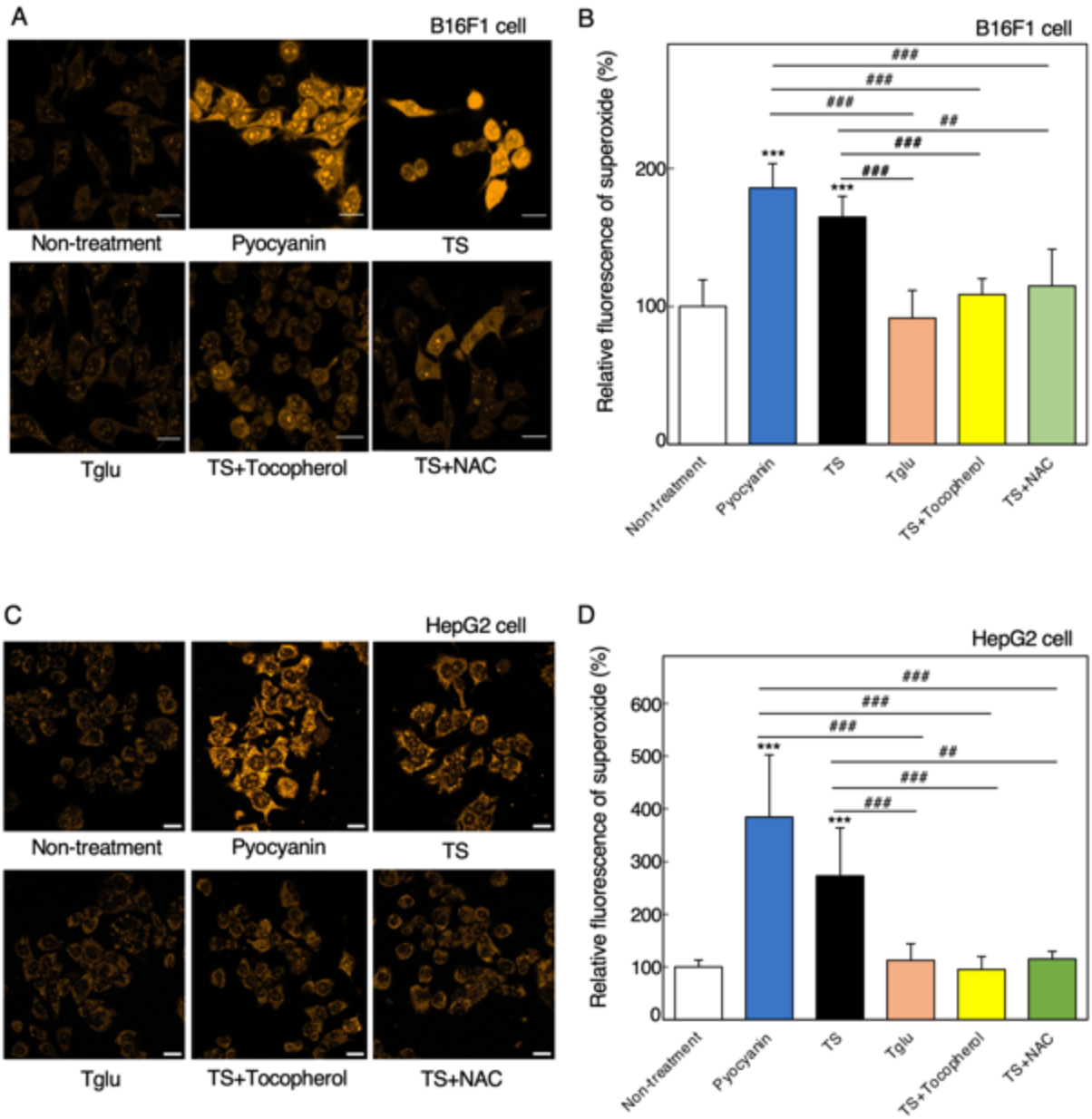

Fig. 2.5 Effects of TS and Tglu on intracellular superoxide production

(A) Intracellular superoxide production in B16F1 cells was detected with a superoxide-activated fluorophore (orange). (B) The fluorescence intensities in B16F1 cells were quantified with ImageJ. (C) Superoxide production in HepG2 cells (D) The fluorescence intensities in HepG2 cells were quantified with ImageJ. Data are shown as mean ± SD (n = 6). ** $P < 0.01$, *** $P < 0.001$ relative to untreated; # $P < 0.05$, ### $P < 0.001$ (one way ANOVA; Tukey's Post hoc test). Scale bar = 20 μm.

2.3.6 Effects of TS and Tglu on intracellular Ca^{2+}

A key mechanism that has been proposed to explain the pro-apoptotic activity of TS is the induction of ER stress (*Huang X, 2010; Huang X, 2013*). Therefore, I compared the effects of TS and Tglu on ER stress by evaluating changes in cytoplasmic Ca^{2+} levels, as increased cytoplasmic calcium is a well-known consequence of ER stress (*Deniaud A, 2007; Galluzzi L, 2014; Shen L, 2016*). Using an assay based on a calcium-activated cell-permeable dye, intracellular calcium was detected in the cytoplasm of B16F1 after 48 h of TS and Tglu treatment (Fig. 2.6). Treatment with TS, however, resulted in increased fluorescence. In contrast, treatment with Tglu correlated with decreased calcium-stimulated fluorescence relative to control and TS-treated cells. Upon quantifying the fluorescence intensity by image analysis, I found that the fluorescence in TS-treated cells was around 202% of that of control in B16F1 cells (Fig. 2.6B). Conversely, the fluorescence intensity of Tglu-treated B16F1 cells was around 52% that of control cells.

IP_3R is the main Ca^{2+} release channel among the calcium releasing channels on ER (*Kania E, 2017*). To examine the involvement of IP_3R in TS-induced calcium release, I treated the cells with both IP_3R antagonist 2-APB (2-Aminoethyl diphenyl borinate) and TS. I found that cells treated with both 2-APB and TS exhibited fluorescence of around 126% (Fig. 2.6B). Again, cells treated with 2-APB alone showed reduced fluorescence of about 77% of that of control. However, the reduction was not statistically significant when compared to the control.

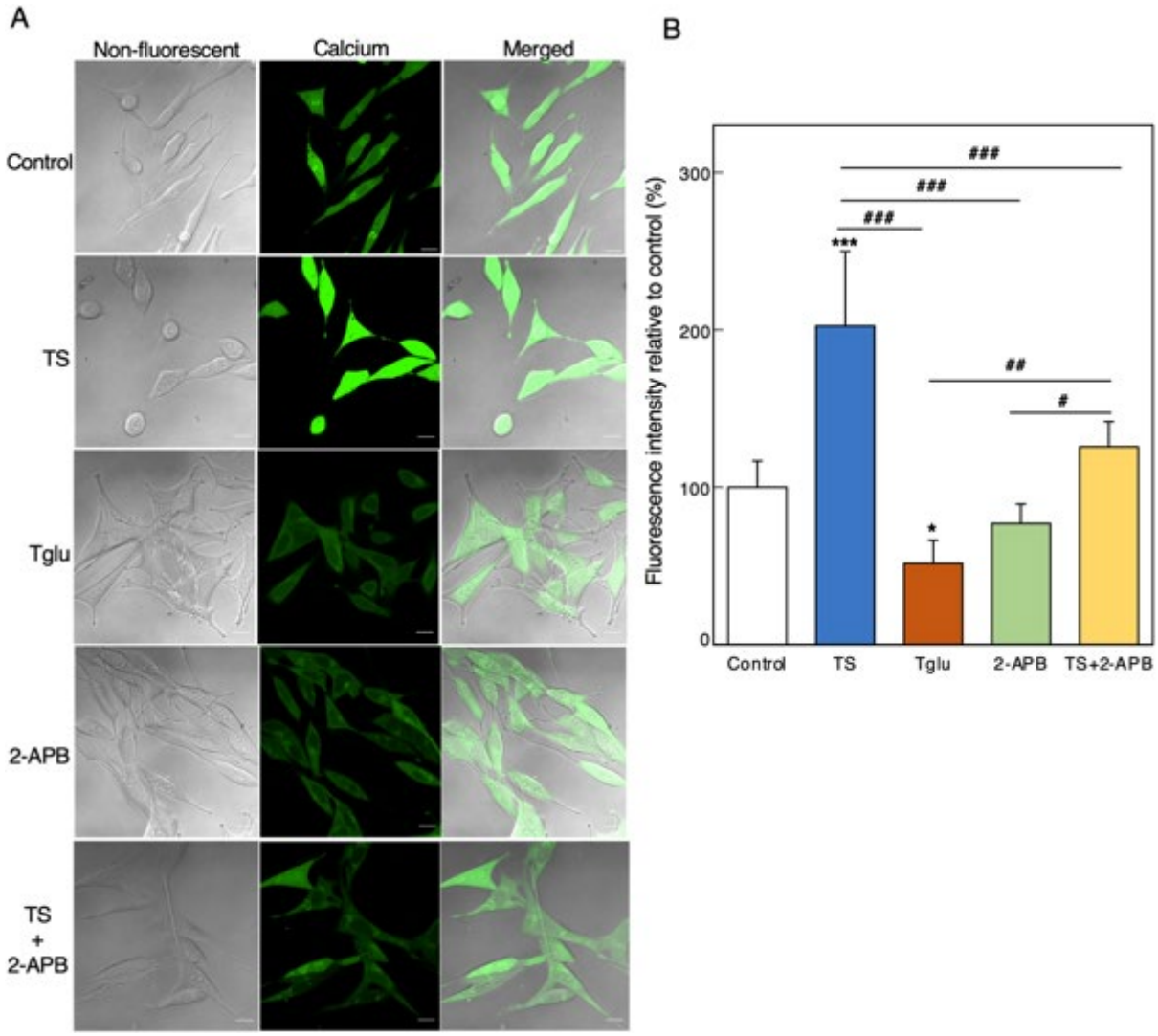

Fig. 2.6 Effects of TS and Tglu on intracellular Ca^{2+}

(A) A fluorescent indicator (Fluo4) was used to detect intracellular Ca^{2+} in B16F1 cells after 48 h of treatments. (B) The fluorescence intensity was quantified by ImageJ. Data are shown as mean ± SD (n = 5). * $P < 0.05$, *** $P < 0.001$ relative to control; # $P < 0.05$, ## $P < 0.01$, ### $P < 0.001$ (one way ANOVA; Tukey's Post hoc test). Scale bar = 20 μm.

2.3.7 Effects of α-tocopherol on intracellular Ca^{2+}

I found that the intracellular amount of Tglu was 22% (Fig. 2.4). I assumed some of the Tglu was hydrolysed to α-tocopherol. Therefore, I compared the effects of α-tocopherol and Tglu on ER stress by evaluating changes in cytoplasmic Ca^{2+} levels. Using an assay based on a calcium-activated cell-permeable dye, intracellular calcium was detected in the cytoplasm of B16F1 after 48 h of α-tocopherol and Tglu treatment (Fig. 2.7). Treatment with 50 μM and 75 μM α-tocopherol did not show any change in Ca^{2+} specific fluorescence compared to control. In contrast, treatment with 75 μM Tglu correlated with decreased calcium-stimulated fluorescence relative to control and 50 μM and 75 μM α-tocopherol treated cells. However, 100 μM α-tocopherol treated cells exhibited fluorescence similar to 75 μM Tglu treated cells. Upon quantifying the fluorescence intensity by image analysis, I found that the fluorescence in 50 μM and 75 μM Tglu-treated cells were around 90% and 80% of that of control in B16F1 cells (Fig. 2.7B). Conversely, the fluorescence intensity of 75 μM Tglu-treated B16F1 cells was around 54% that of control cells. In addition, 100 μM α-tocopherol decreased fluorescence intensity to 57% that of control.

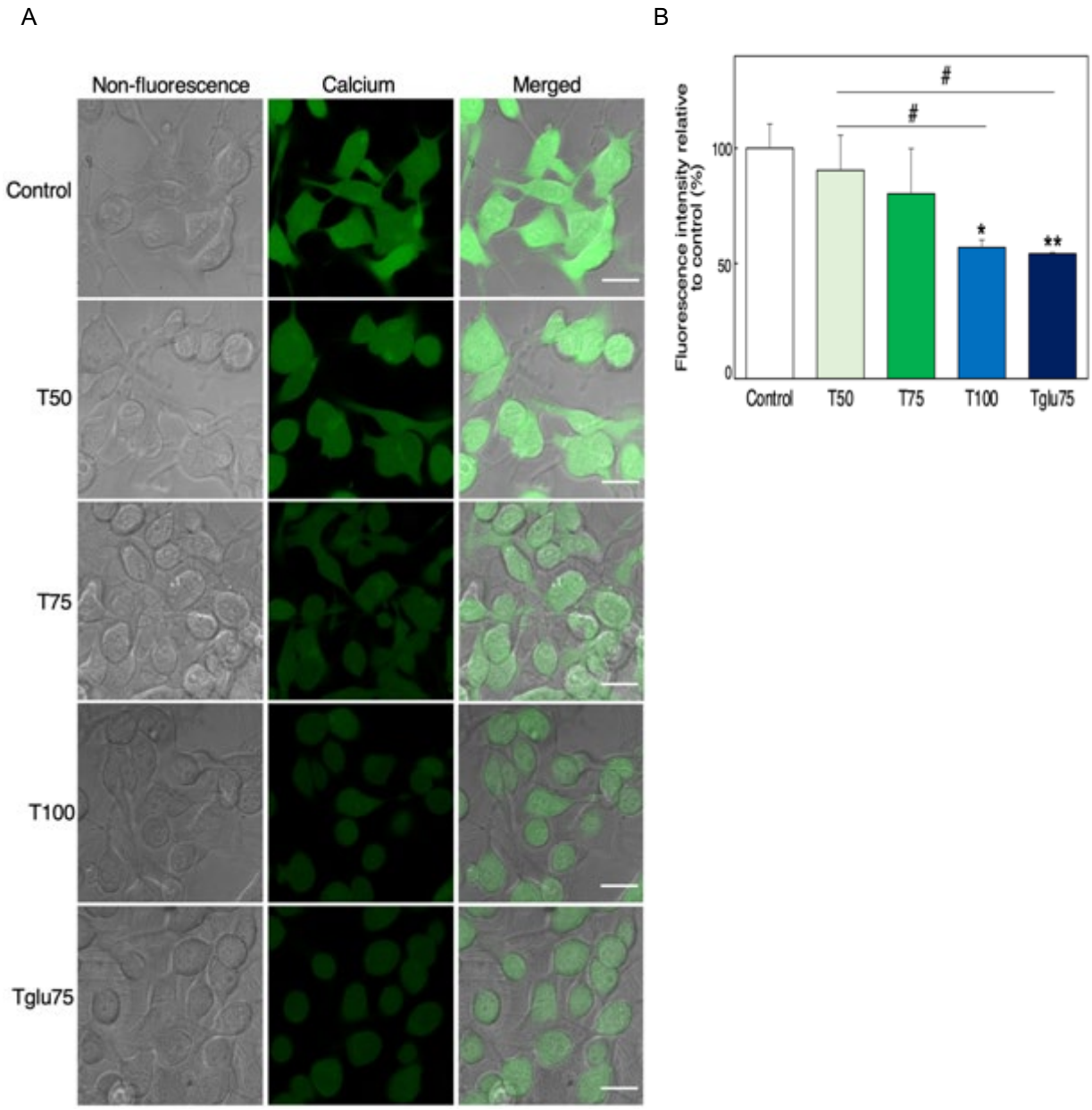

Fig. 2.7 Effects of α-Tocopherol on intracellular Ca^{2+}

(A) A fluorescent indicator (Fluo4) was used to detect intracellular Ca^{2+} in B16F1 cells after 48 h of treatments. (B) The fluorescence intensity was quantified by ImageJ. Data are shown as mean ± SD (n = 3). * $P < 0.05$, ** $P < 0.01$ relative to control; # $P < 0.05$ (one way ANOVA; Tukey's Post hoc test). T50, T75 and T100 indicate 50 μM, 75 μM and 100 μM α-tocopherol respectively. Tglu75 indicates 75 μM Tocopheryl glutarate. Scale bar = 20 μm.

2.3.8 Effect of TS on intracellular Ca^{2+} in Ca^{2+} free cell culture medium

To investigate the source of Ca^{2+} in TS-induced elevation of intracellular Ca^{2+} level, I treated B16F1 cells with 75 μM TS containing liposomes in Ca^{2+} free cell culture medium to exclude the possibility of Ca^{2+} influx from outside the cell. After 6 h of TS treatment, intracellular calcium was detected using calcium-activated cell-permeable dye (Fig. 2.8). Treatment with TS resulted in increased Ca^{2+} stimulated fluorescence relative to control, while combined treatment of TS and 2-APB reduced fluorescence to control level. The quantification of fluorescence intensity by image analysis, I found that the fluorescence in TS-treated cells was approximately 148% of that of control (Fig. 2.8B). Notably, cells treated with both TS and 2-APB exhibited fluorescence that was similar to that exhibited by control cells.

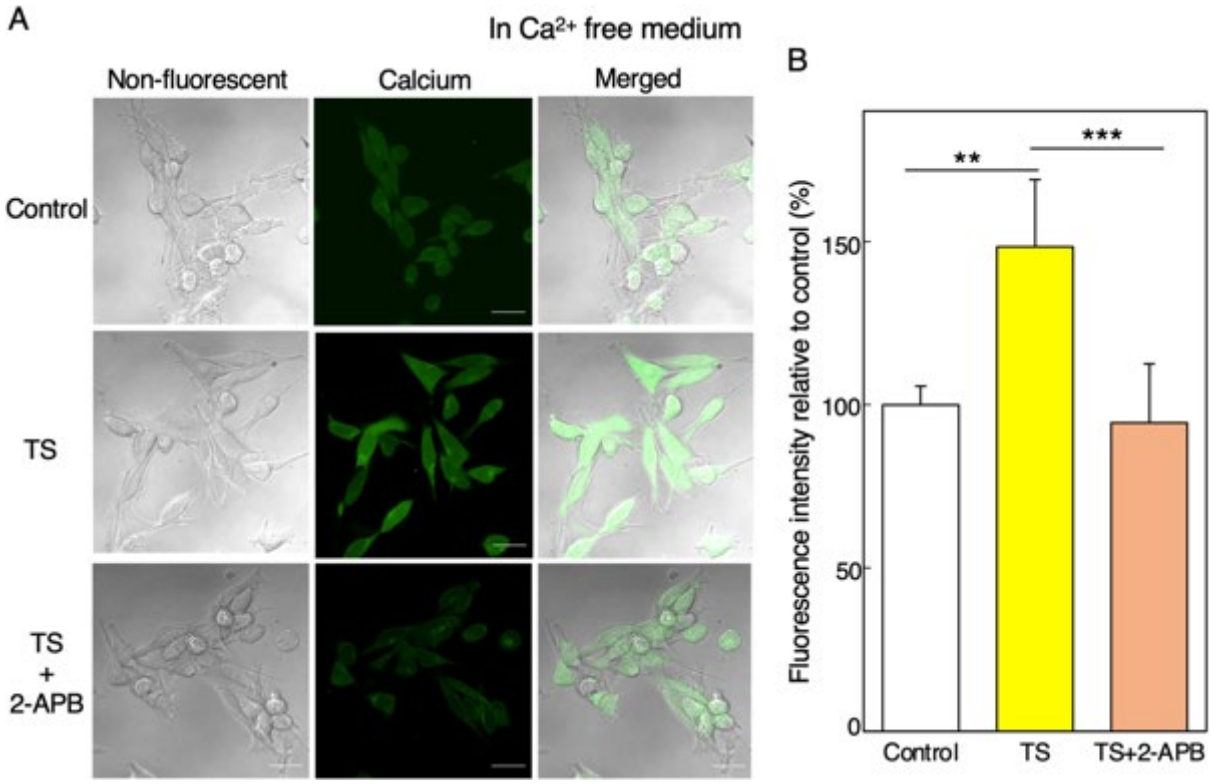

Fig. 2.8 Effect of TS on intracellular Ca^{2+} in Ca^{2+} free cell culture medium
(A) A fluorescent indicator (Fluo4) was used to detect intracellular Ca^{2+} in B16F1 cells after 6 h of 75 μM TS treatment in Ca^{2+} free culture medium (B) The fluorescence intensity was quantified by ImageJ. Data are shown as mean ± SD (n = 5). ** $P < 0.01$, *** $P < 0.001$ (one way ANOVA; Tukey's Post hoc test). Scale bar = 20 μm.

2.3.9 Effect of 2-APB on TS-induced cytotoxicity *in vitro*

Based on the result of TMRE fluorescence restoration by 2-APB in TS-treated cells, I investigated the effect of 2-APB on TS-induced cytotoxicity by treating the cells for 48 h with either different concentrations of 2-APB or a combination of 75 µM TS and different concentrations of 2-APB. I found that 2-APB is non-cytotoxic as measured by trypan blue exclusion assays (Fig. 2.9A). However, pre-treatment with 2-APB for 1 h was found to improve cell viability in both TS-treated B16F1 and HepG2 cells in a dose-dependent manner (Fig. 2.9B, C). TS treatment decreased cell viability to around 72% in B16F1 cells, while 25 µM and 50 µM 2-APB increased cell viability to about 78% and 89% relative to control, respectively, in TS-treated B16F1 cells. In addition, TS treatment decreased cell viability to around 65% that of control in HepG2 cells. Conversely, I found 73% cell viability in HepG2 cells treated with both 25 µM 2-APB and 75 µM TS, while cell viability was 85% in cells treated with both 50 µM 2-APB and 75 µM TS.

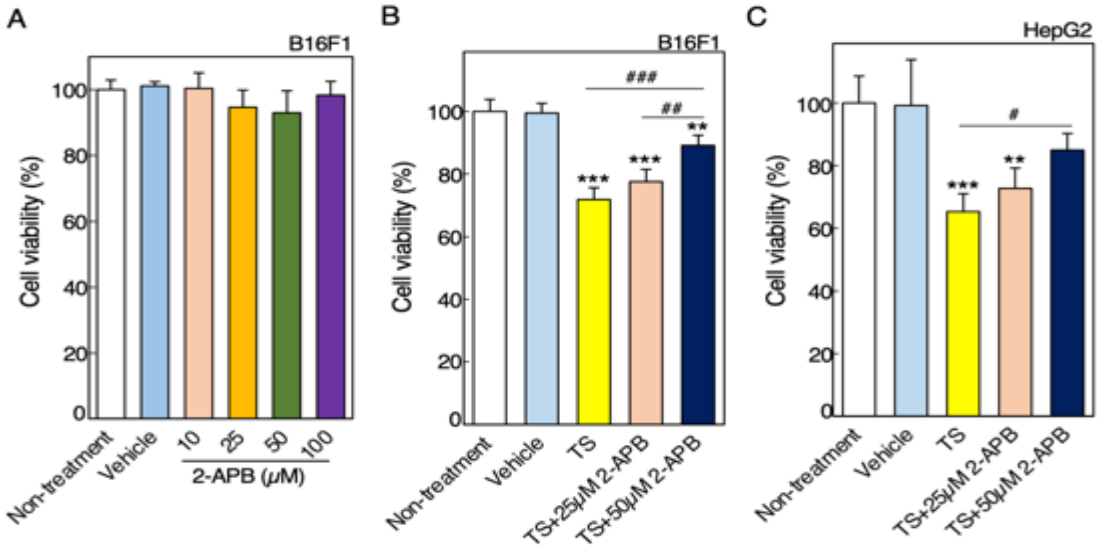

Fig. 2.9 Effect of 2-APB on TS-induced cytotoxicity *in vitro*

B16F1 cells were treated with different concentrations of 2-APB in dimethyl sulfoxide (DMSO) for 48 hr. Cell viability was measured by trypan blue exclusion assay. (A) Viability of B16F1 cells after 2-APB treatment for 48 h. B16F1 and HepG2 cells were treated with 25 µM and 50 µM 2-APB for 1 h prior to addition of 75 µM TS-containing liposome. (B) Viability of B16F1 cells treated with both 2-APB and TS (C) Viability of HepG2 cells treated with both 2-APB and TS. Data are shown as mean ± SD (n = 6). ** $P < 0.01$, *** $P < 0.001$ vs control, # $P < 0.05$; ## $P < 0.01$; ### $P < 0.001$ (one way ANOVA; Tukey's Post hoc test).

2.3.10 Effects of TS treatment on GRP78 protein

GRP78 initiates adaptive responses to protect cells from ER stress-induced apoptosis (*Wu Y, 2005; Booth L, 2012; Dauer P, 2019; Ibrahim IM, 2019*), providing a potential mechanism whereby TS and Tglu may modulate ER stress.

To analyze the expression of GRP78 on normal cells (mouse 3T3-Swiss albino) and untreated cancer cells, I used real-time PCR to quantify the mRNA expressed from the *HSP5A* gene, which encodes for GRP78. The RT-PCR signal from GRP78 mRNA was normalized to that of the housekeeping gene *GAPDH* and *β-actin* so as to control for cytotoxic effects. I found that the GRP78 mRNA is higher in B16F1 cells compared to mouse 3T3-Swiss albino cells (Fig. 2.10A-2.10C). The GRP78 mRNA in B16F1 cells was around 190% of that of mouse 3T3-Swiss albino cells. I also assessed GRP78 protein expression by western blotting. I found higher expression of GRP78 protein in B16F1 cells compared to 3T3-Swiss albino cells (Fig. 2.10A). Quantification of western blot band intensities by image analysis showed that GRP78 band intensity was about 250% that of mouse 3T3-Swiss albino cells.

I examined the GRP78 protein level in TS-treated B16F1and HepG2 cells. I found that GRP78 protein decreased in a time-dependent manner in TS-treated cells (Fig. 2.10D, 2.10G). Quantification by image analysis revealed that the intensity of the GRP78 band from TS-treated B16F1 cells was around 71% that of control after 12 h, 63% that of control after 24 h, and 47% that of control after 48 h (Fig. 2.10E). In addition, GRP78 band intensity was around 90% that of control after 12 h, 45% that of control after 24 h, and 66% that of control after 48 h (Fig. 2.10H) in TS-treated HepG2 cells.

To investigate the underlying mechanism of TS-induced GRP78 downregulation in the cancer cells, we quantified the GRP78 mRNA level by real-time PCR. As shown in Fig. 2.10F, treatment with TS correlated with a decrease of GRP78 mRNA in B16F1 cells relative to that in untreated control cells in a time-dependent manner. Specifically, after 24 h of treatment, TS suppressed GRP78 mRNA to around 64% of that of control. After 48 h, GRP78 mRNA was suppressed to around 37% of the control level in TS-treated B16F1 cells. The degree of suppression of GRP78 mRNA by TS was significantly higher after 48 h as compared to the effect at 24 h. However, in the case of HepG2 cells, 24 h of TS treatment increased GRP78 mRNA to around 198% that of control, while after 48 h, GRP78 mRNA decreased to the control level (Fig. 2.10I).

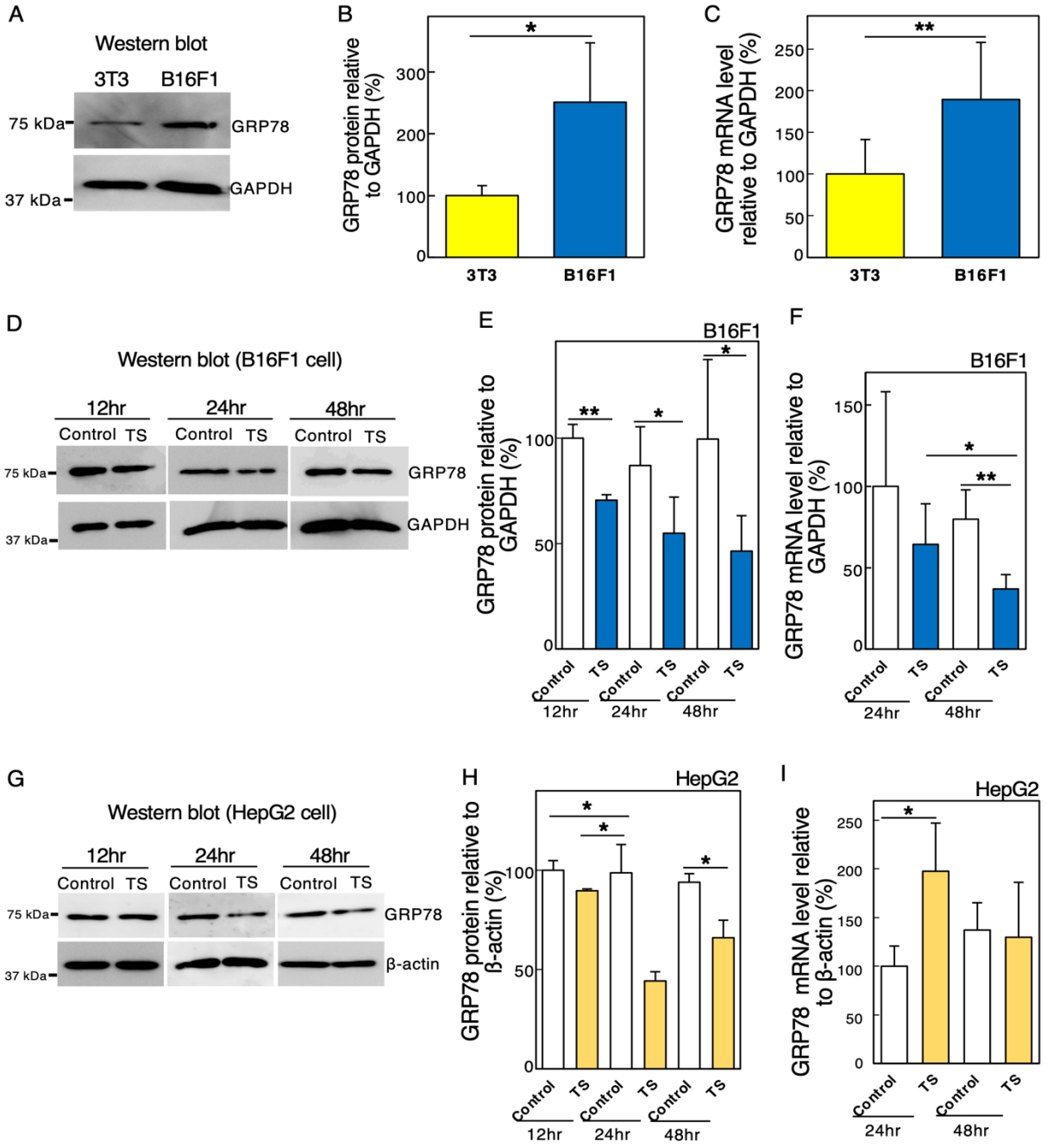

Fig. 2.10 Effect of TS on GRP78 expression

B16F1 and HepG2 cells were treated with 75 μM TS-containing liposomes. The whole-cell lysate was collected from control cells and cells treated with 75 μM TS-containing liposomes after three-time points (12, 24, and 48 h), and Western blotting was performed, with GAPDH and β-actin serving as an internal control. The intensities of protein bands were quantified by ImageJ. (A) GRP78 protein bands in untreated mouse 3T3-Swiss albino and B16F1 cells (B) Quantification of western blot band intensities. (D, E) GRP78 protein bands and quantification in TS treated B16F1 cells. (G, H) GRP78 protein bands and

quantification in TS treated HepG2 cells. Total RNA was isolated 24 and 48 h after treatment, and quantitative real time-PCR was performed (n = 5). Shown are levels of GRP78 mRNA relative to that of the housekeeping gene *GAPDH or β-actin*. Quantification of GRP78 mRNA in (C) untreated mouse 3T3-Swiss albino and B16F1 cells, (F) TS treated B16F1 cells, (I) TS treated HepG2 cells. Data are shown as mean ± SD (n = 5). * $P < 0.05$, ** $P < 0.01$ (unpaired Student's t-test; one way ANOVA; Tukey's Post hoc test).

2.3.11 Effects of Tglu and α-tocopherol treatment on GRP78 protein

I also examined the effect of Tglu and α-tocopherol treatment on GRP78 protein expression. Results of Western blotting assays demonstrated that GRP78 protein increased over time in Tglu treated cells (Fig. 2.11A and D) while no change in GRP78 protein level observed in α-tocopherol treated cells compared to control cells (Fig. 2.11G-H).

Specifically, quantification of band intensities by image analysis showed that GRP78 increased significantly in Tglu-treated B16F1 cells to around 172% and 137% relative to control after 24 h and 48 h, respectively (Fig. 2.11B). In contrast, Tglu treatment initially decreased GRP78 protein after 12 h of treatment, but after 24 h, it increased GRP78 band intensity to around 147% that of control and 117% that of control after 48 h in HepG2 cells (Fig. 2.11E).

As shown in Fig. 2.11C and 2.11F, treatment with Tglu induced time-dependent and significant increases in GRP78 mRNA relative to control in both B16F1 and HepG2 cells. 24 h of Tglu treatment induced significant increases in GRP78 mRNA to around 119% in B16F1 cells and around 149% in HepG2 cells compared to control. In addition, GRP78 mRNA level increased to around 146% that of control in Tglu-treated B16F1 cells, while 48 h of Tglu treatment induced around 126% increase in GRP78 mRNA level compared to control in HepG2 cells.

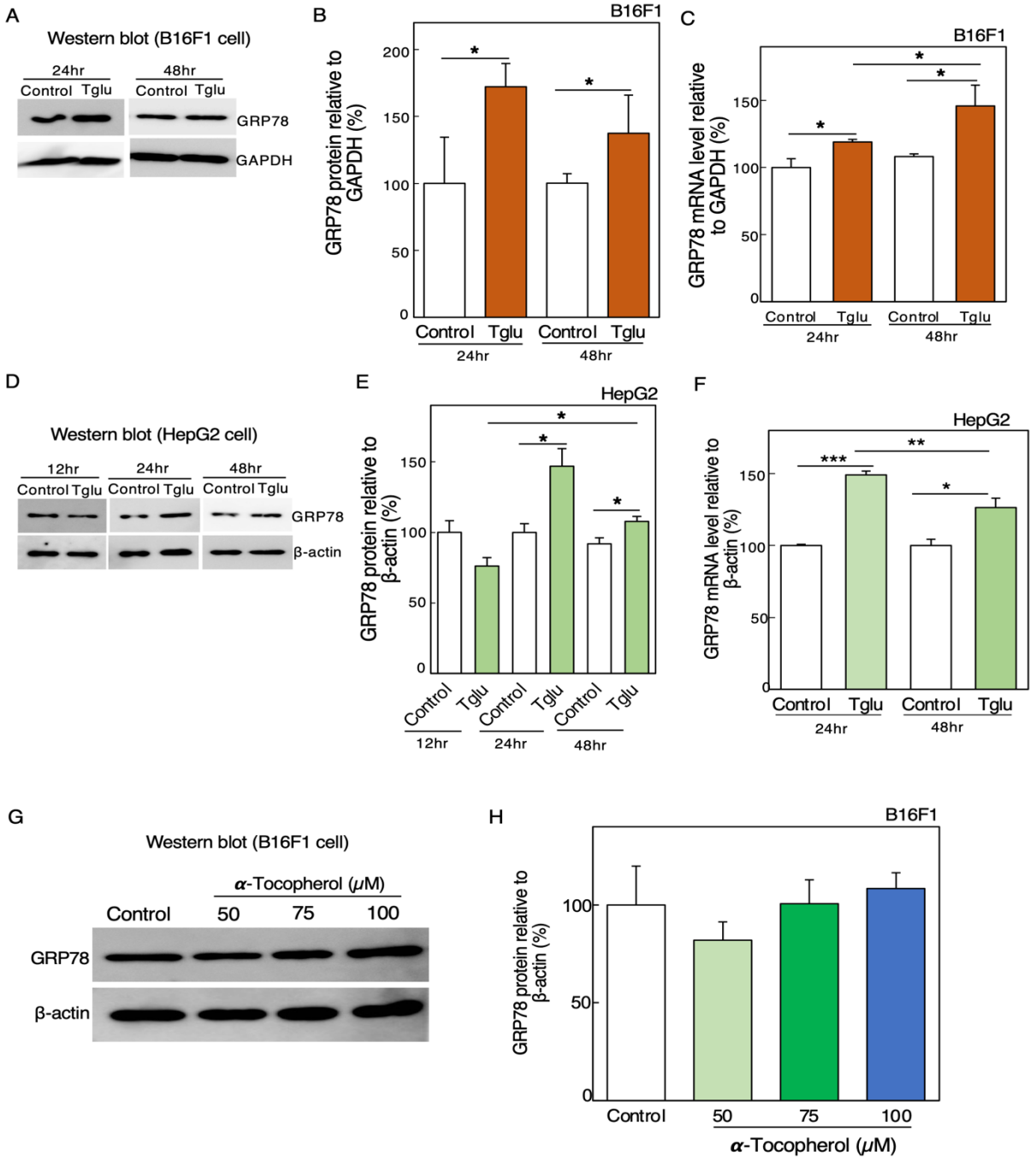

Fig. 2.11 Effect of Tglu and α-tocopherol on GRP78 expression

B16F1 and HepG2 cells were treated with 75 μM Tglu-containing liposomes and different concentrations of α-tocopherol. The whole-cell lysate was collected from control cells and cells treated with 75 μM Tglu-containing liposomes and Western blotting was performed, with GAPDH and β-actin serving as an internal control. The intensities of protein bands were quantified by ImageJ. (A, B) GRP78 protein bands and quantification in Tglu treated B16F1 cells. (D, E) GRP78 protein bands and quantification in Tglu treated HepG2 cells. (G, H) GRP78 protein bands and

quantification in α-tocopherol treated B16F1 cells. Total RNA was isolated 24 and 48 h after treatment, and quantitative real time-PCR was performed (n = 5). Shown are levels of GRP78 mRNA relative to that of the housekeeping gene *GAPDH or β-actin*. Quantification of GRP78 mRNA in (C) Tglu treated B16F1 cells, (F) Tglu treated HepG2 cells. Data are shown as mean ± SD (n = 5). * $P < 0.05$, ** $P < 0.01$, *** $P < 0.001$ (one way ANOVA; Tukey's Post hoc test).

2.3.12 Localization of GRP78 after TS and Tglu treatment

Generally, GRP78 is thought to reside in the lumen of ER; however, it also shows a diffuse distribution throughout the cytoplasm (*Sun FC, 2006*). To investigate the changes in GRP78 localization between ER and cytoplasm upon TS and Tglu treatment, I performed immunostaining using anti-calreticulin antibody as the marker of ER lumen. GRP78 was detected as green fluorescence and calreticulin as red fluorescence in B16F1 after 48 h of TS and Tglu treatment (Fig. 2.12). Here, the yellow signal in merged images represents the localization of GRP78 in the lumen of ER. However, TS-treated B16F1 cells showed decreased yellow fluorescence compared to control, while yellow fluorescence was higher in Tglu-treated cells. The ratio of yellow fluorescence to total green fluorescence calculated by the colour thresholding method of image analysis revealed that in control cells, the ratio was about 48% (Fig. 2.12B). On the other hand, the ratio was 17% in TS-treated cells. In accord with previous results, the opposite effect was observed upon treatment with Tglu: Tglu treatment increased the ratio of yellow to total green signal to about 62%.

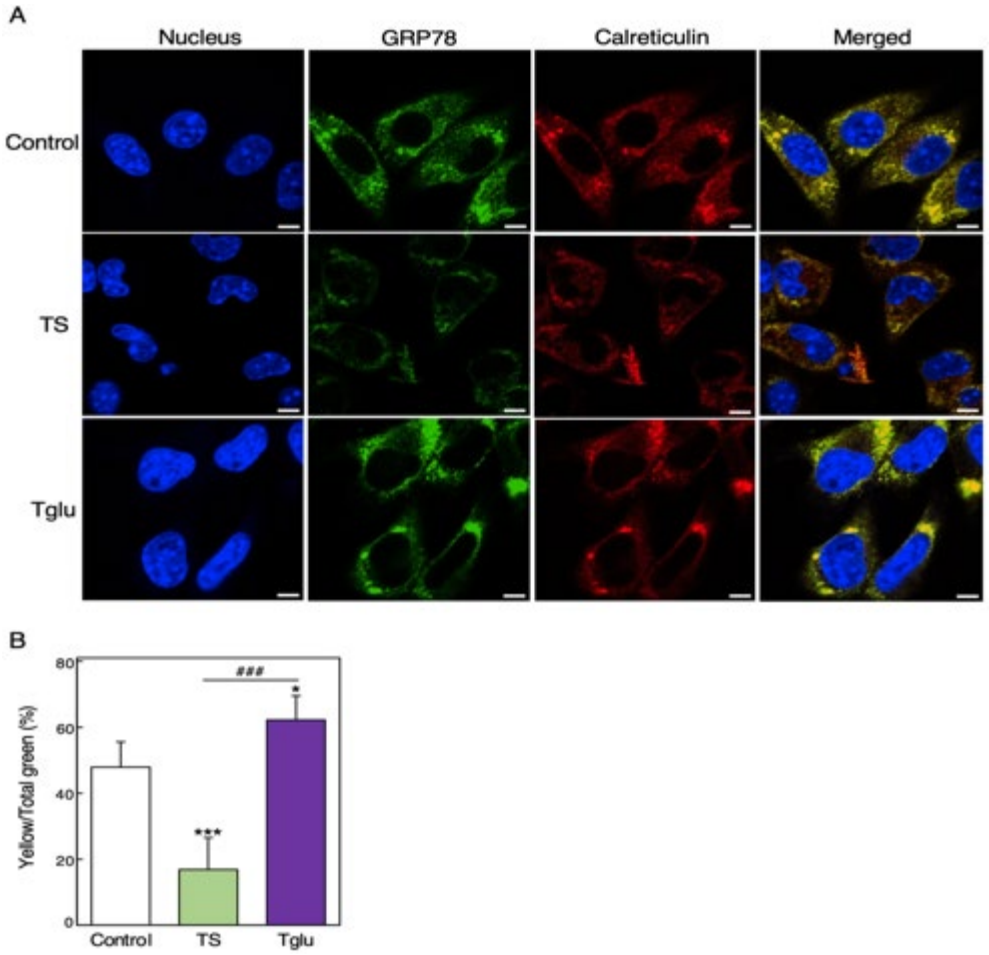

Fig. 2.12 Effects of TS and Tglu on GRP78 localization

B16F1 cells were separately treated with 75 μM TS- and Tglu-containing liposomes for 48 h. Cells were fixed and permeabilized prior to immunostaining with an anti-GRP78 antibody and an Alexa Fluor 488-conjugated secondary antibody. Next, cells were immunostained with an anti-calreticulin antibody and an Alexa Fluor 647-conjugated secondary antibody. Nuclei were counterstained with DAPI (blue). (A) GRP78 (green) and calreticulin (Red) were observed after the noted treatments. Yellow fluorescence in the merged images represents colocalization of GRP78 and calreticulin (B) Percent ratio of yellow signal to total green signal. Data are shown as mean ± SD (n = 5). *, $P < 0.05$, ***, $P < 0.001$ relative to control; ###, $P < 0.001$ (one way ANOVA; Tukey's Post hoc test). Scale bar = 20 μm.

2.4 Discussion

It was reported that the terminal dicarboxylate moiety must contain four or less than four carbon atoms in order for a derivative of α-tocopherol to display pro-apoptotic activity (*Kogure K, 2004*). However, the relation between structural changes in the terminal dicarboxylate moiety and biological activities of the tocopheryl ester derivatives leading to pro-apoptotic activity has not been elucidated yet. In the present study, I studied the effect of changes in the side chain length at the terminal ester moiety of the tocopheryl esters on their pro-apoptotic activity.

TS caused cytotoxicity in B16F1 cells (Fig. 2.1A), human hepatic carcinoma HepG2 cells (Fig. 2.1B) and mouse 3T3-Swiss albino cells (Fig. 2.1C). However, the higher cytotoxicity of TS in B16F1 and HepG2 cells compared to mouse 3T3-Swiss albino cells indicates that the cancer cells are more sensitive to TS treatment than normal cells. Previously we have shown the higher sensitivity of cancer cells toward TS treatment is due to the failure of their antioxidative defence system (*Kogure K, 2002*). As shown in Fig. 2.1D, TS-induced morphological changes of the nucleus characterized by the formation of the apoptotic bodies confirm cellular apoptosis upon TS treatment.

In contrast, Tglu, with a single additional carbon in the terminal ester (Fig. 1.2), was not cytotoxic to B16F1 and HepG2 cells (Fig. 2.1E and 2.1F). These results suggest that an increase in carbon number from four to five in the terminal ester group of tocopheryl esters diminishes the cytotoxic effect. I investigated this interesting phenomenon to identify the underlying mechanisms.

TS has been reported to preferentially accumulate in the mitochondria of the hepatocytes (*Dos Santos GAS, 2011*). However, the possibility of accumulation of TS to other organelle is not excluded. Again, it is well established that TS interferes with the activities of mitochondrial respiratory chain components and generates superoxide (*Kang YH, 2004; Neuzil J, 2006; Dong LF, 2008; Dos Santos GAS, 2011; Rauchová H, 2014*). Taken together, I hypothesized that accumulation of the generated superoxide by TS may cause oxidative stress leading to ER stress. In this current study, I found that TS downregulated ER residing chaperone protein GRP78 (Fig. 2.10), suggesting the possibility of ER as another target organelle of TS. I think the hydrophobic nature of TS may allow its distribution between lipid membranes of other organelles. Therefore, the primary target organelle of TS is unknown.

My current study confirmed superoxide generation by TS using superoxide specific fluorescence probe, which is insensitive to other peroxide, hydroxyl radical, peroxynitrite, chlorine and bromine species. The quantification of fluorescence intensity showed that TS

significantly increases superoxide production in B16F1 and HepG2 cells (Fig. 2.5) as compared to untreated cells. At the same time, α-Tocopherol and NAC-treatment significantly reduced TS-induced superoxide production (Fig. 2.5B and 2.5D). α-Tocopherol and NAC-treatment may prevent leakage of electron from mitochondrial respiratory chain and thereby prevents the superoxide generation (*Chow CK, 2001; Martinez BM, 2000*) . Importantly, though, the newly synthesized tocopheryl ester, Tglu, did not generate superoxide like TS does, lending support to the conclusion that Tglu is less cytotoxic than TS. These findings further suggest that the structural change in the ester moiety drastically affects the superoxide generation by the tocopheryl esters.

ROS generation has also been demonstrated to cause ER stress, which leads to apoptosis in human gastric cancer cells (*Huang X, 2010; Huang X, 2013*). The ER lumen has a highly regulated microenvironment consisting of molecular chaperones and folding enzymes and high concentrations of ATP and Ca^{2+} (*Görlach A, 2015*). Changes in these components may alter ER homeostasis, leading to ER stress (*Krebs J, 2015*), which is characterized by increased cytoplasmic Ca^{2+} (*Lebeau PF, 2021*). In addition, superoxide may induce Ca^{2+} release from ER by inhibiting the degradation process of inositol 1,4,5-triphosphate (IP_3) protein, a ligand of the main Ca^{2+} releasing channel IP_3R on ER (*Suzuki YJ, 1992; Kania E, 2017*). Hence, taking the superoxide generation ability by TS into account, I hypothesized TS might induce Ca^{2+} release by indirectly stimulating IP_3R. To test my hypothesis, I examined intracellular Ca^{2+} level upon TS, Tglu and 2-APB (IP_3R antagonist) treatment in B16F1 cells. I found that TS-treated B16F1 exhibited increased cytoplasmic Ca^{2+} (Fig. 2.6), suggesting induction of ER stress in B16F1 cells. In addition, a significant reduction in cytoplasmic Ca^{2+} in cells treated with both TS and IP_3R antagonist 2-APB compared to TS-treated cells support TS-induced Ca^{2+} release through the IP_3R channel. Conversely, Tglu treatment actually decreased Ca^{2+}-specific fluorescence, suggesting that Tglu may compensate for, rather than cause, ER stress. Furthermore, TS-treated cells exhibited higher Ca^{2+}-specific fluorescence relative to control in Ca^{2+}-free cell culture medium, while 2-APB treatment restores TS-induced elevation of Ca^{2+} to the control level (Fig. 2.8). This finding confirms ER as the source of Ca^{2+} in TS-induced Ca^{2+} inflation.

In either event, the increased cytoplasmic Ca^{2+} may cause mitochondrial Ca^{2+} overload, with accompanying mitochondrial swelling, perturbation or rupture of the outer membrane, and release of apoptotic factors (*Giorgi C, 2012*). The immunoassay of cytochrome c showed that cytochrome c and MitoTracker signal overlapped in control cells. The cytofluorogram obtained from the control cells (Fig. 2.2B) by using “co-localization finder” of ImageJ represents linear

co-relation between cytochrome c and MitoTracker signal. The Pearson coefficient of 0.99 suggests perfect localisation of cytochrome c in the mitochondria of the control cells. On the other hand, the cytofluorogram obtained from TS-treated cells did not represent a linear co-relation between cytochrome c and MitoTracker signal (Fig. 2.2C). The Pearson coefficient value of 0.45 represents a lack of overlapping between cytochrome c (green) and MitoTracker (red) signal indicating that cytochrome c is no longer in the mitochondria. This finding suggests cytochrome c release due to mitochondrial membrane rupture upon TS treatment.

Again, the loss of mitochondrial integrity is associated with mitochondrial depolarization. I confirmed mitochondrial depolarization in TS-treated B16F1 and HepG2 cells (Fig. 2.3). Notably, 2-APB treatment restored mitochondrial membrane potential loss induced by TS in both cells suggesting the involvement of Ca^{2+} leakage from ER in mitochondrial depolarization (Fig. 2.3C and 2.3D). In addition, we found that blocking of Ca^{2+} leakage by pre-treatment with 25 μM and 50 μM 2-APB dose-dependently improves cell viability in TS-treated B16F1 (Fig. 2.9B) and HepG2 cells (Fig. 2.9C). These findings suggest that Ca^{2+} overload on mitochondria due to TS induced Ca^{2+} leakage from ER is responsible for TS-induced apoptosis and demonstrates a crucial relationship between ER and mitochondria in apoptosis induction.

Oxidative stress induction by TS may damage intracellular proteins structurally, resulting in the accumulation of misfolded proteins and, consequently, ER stress. Chaperone proteins play a vital role in managing these misfolded proteins and reestablishing ER homeostasis. GRP78 is an essential chaperone that acts as a Ca^{2+} buffer in the lumen of the ER (*Prins D, 2011*). GRP78 also maintains mitochondrial functionality by reducing Ca^{2+} efflux from the ER to mitochondria and by managing misfolded mitochondrial proteins and mitochondrial steroidogenesis (*Ouyang YB, 2011; Prasad M, 2017; Nowicka U, 2021*). Recently, it has been proposed that GRP78 overexpression aids neuroprotection by triggering the mitophagy process (*Leiva-Rodríguez T, 2021*). The real-time PCR and western blotting results confirm that GRP78 activity is higher in B16F1 cells than mouse 3T3-Swiss albino cells (Fig. 2.10A-C), providing an important link between GRP78 expression and cancer cell survival under hostile conditions. Furthermore, downregulation of GRP78 has been proposed to cause apoptosis in several types of cancer cells (*Booth L, 2012; Yun S, 2017; Kao C, 2018; Liang G, 2018; Yu X, 2018; Sharma SH, 2018; Martucciello, 2018; Dauer P, 2019*). Thus, the role of GRP78 in maintaining ER stress homeostasis and mitochondrial functionality suggests important relationships among downregulation of GRP78, ER stress, mitochondrial dysfunction, and apoptosis in cancer cells. I found that TS downregulates GRP78 expression in both B16F1 and HepG2 cells (Fig. 2.10D, 2.10E and Fig. 2.10G, 2.10H). Not only that decreased ratio of luminal GRP78 to total GRP78

in TS-treated cells indicates a loss of GRP78 in the ER lumen (Fig. 2.12). Hence, TS may negatively affect protein folding and, consequently, Ca^{2+} homeostasis in the lumen of the ER, contributing to Ca^{2+} leakage from the ER into the cytoplasm. Taken together, GRP78 downregulation by TS might be one of the key events in the induction of ER stress and mitochondrial depolarization that lead to apoptosis. However, it is still inconclusive whether TS indirectly causes ER stress via superoxide generation or directly induces ER stress by downregulating GRP78. Further investigation is required to find out the trigger of ER stress-induced by TS.

On the other hand, Tglu treatment was found to upregulate GRP78 expression in B16F1 and HepG2 cells (Fig. 2.11A-2.11F). Tglu-treated cells were found with an increased amount of GRP78 in the ER lumen (Fig. 12A, B). Thus, upregulation of GRP78 by Tglu may support ER homeostasis by decreasing the amount of intracellular misfolded proteins and preventing Ca^{2+} leakage from the ER. The reduced cytoplasmic Ca^{2+} in Tglu-treated B16F1 (Fig. 2.6A, B) is consistent with this model. These results further support the inhibition of ER stress by Tglu. Through this mechanism, Tglu would protect mitochondria from intracellular Ca^{2+} overload, thereby leading to a non-cytotoxic character. The increase of mitochondrial fluorescence in TMRE assay upon Tglu-treatment (Fig. 2.3) and cytotoxicity results (Figs. 2.1E and 2.1F) support this statement.

Next, I have confirmed the transfer of TS and Tglu from the cell culture medium to the cell. As shown in Fig. 2.4A, almost all the applied TS transferred to cells. On the other hand, the intracellular presence of 23% and 20% of applied Tglu remaining in the cell culture medium after 24 h indicates around 57% of applied Tglu disappeared from the cell culture medium and cell. It suggests that the possibility of the hydrolysis of Tglu in the cell in my experimental condition (Fig. 2.4B). These findings suggests that TS is less prone to hydrolysis than Tglu. I assumed the possibility of conversion of Tglu into α-tocopherol. Hence, I examined the effect of α-tocopherol on intracellular Ca^{2+} level and GRP78 expression. I found that 50 μM and 75 μM α-tocopherol did not affect intracellular Ca^{2+} level (Fig. 2.7). However, 100 μM α-tocopherol showed almost similar reduction in intracellular Ca^{2+} level compared to 75 μM Tglu (Fig. 2.7B). In addition, α-tocopherol treatment did not affect the GRP78 protein level even at higher dose of 100 μM (Fig. 2.11G and 2.11H). These findings suggest that the Tglu itself caused the inhibition of ER stress. Therefore, HPLC analysis confirms that TS and Tglu reached the intracellular region and initiated opposite biological activities. Furthermore, I investigated the mechanism of GRP78 protein downregulation by TS and upregulation by Tglu.

GRP78 mRNA quantification in the TS-treated cancer cells suggests that TS treatment decreases GRP78 mRNA (Fig. 2.10F and 2.10I). Conversely, Tglu-treated cells have shown an increased level of GRP78 mRNA (Fig. 2.11C and 2.11F). These findings suggest that TS may downregulate GRP78 protein by interfering with the transcription or stability of GRP78 mRNA, while Tglu does the opposite and upregulate GRP78 protein. However, protein synthesis involves a complex interplay of macromolecules like mRNA, tRNA, rRNA and non-ribosomal protein factors. Therefore, GRP78 mRNA reduction by TS does not confirm the target organelle of TS in GRP78 downregulation.

Again, it was observed that GRP78 protein continued to decrease even after 12 h and 24 h of treatment (Figs. 2.10D, E and 2.10G, H). Considering that the half-life of GRP78 is longer than 36 h (*Sugawara S, 1993*), this observation suggests that intracellular degradation systems, such as the ubiquitin-proteasome or autophagy systems, may be activated by TS. Therefore, the mechanism of GRP78 downregulation by TS is not clearly understood. Previously, it was reported that TS directly interacts with and activates protein kinase C (PKC) (*Kogure K, 2004*). Hence, there is a possibility that activation of PKC by TS is correlated with the suppression of GRP78 expression. In addition, some other natural compounds like docosahexaenoic acid, curcumin, and lanatoside C have also been reported to suppress GRP78 expression (*Fasano E, 2012; Feng K, 2019; Ha DP, 2021*). Interestingly, these compounds also activate PKC (*Aires V, 2007; Mahmmoud YA, 2007; Chao MW, 2017*) lending further support to the correlation between the PKC activation and GRP78 downregulation. However, another research group found that the inhibition of PKC suppresses GRP78 mRNA level under hypoxic condition (*Koong AC, 1994*). Therefore, the regulation of GRP78 by PKC is controversial. Further investigation is required to confirm the correlation between activation of PKC by the tocopheryl esters and GRP78 expression.

2.5 Conclusion

A single carbon difference between TS and Tglu resulted in opposing effects on cellular apoptosis, superoxide generation, ER stress induction, and mitochondrial depolarization due to loss of mitochondrial integrity. I also demonstrated the involvement of GRP78 protein in the induction of ER stress by TS and the interplay between ER and mitochondria in TS-induced apoptosis. The structural difference may affect the stability, conformation, or structural flexibility of the tocopheryl esters, affecting their interactions with different molecular targets. Importantly, in this chapter, I demonstrated the flexibility of tocopheryl esters in terms of

biological activities. Nonetheless, I propose a broader potential for the application of tocopheryl esters to the treatment of different diseases, including cancer.

Chapter 3

Investigating the Effect of TS on Endoplasmic Reticulum-Mitochondria contact site

Chapter 3: Investigating the Effect of TS on Endoplasmic Reticulum-Mitochondria contact site

3.1 Introduction

The endoplasmic reticulum-mitochondria contact sites earned much attention of the researcher due to their essential role in lipid and Ca^{2+} homeostasis (*Giacomello M, 2016*). These contact sites also known as mitochondria associated ER membrane (MAM). IP_3R is a ER membrane residing inositol triphosphate-dependent calcium channel is one of the major components of the MAM that controls release of Ca^{2+} from ER to cytoplasm. In addition, IP_3R is involved in several Ca^{2+} dependent cellular processes like proliferation, differentiation, motility, fertilization, survival, autophagy, and apoptosis (*Berridge MJ., 2000; Clapham DE, 2007; Joseph SK, 2007; Ahumada-Castro U, 2021*).

VDAC is another component of MAM. It resides on the outer mitochondrial membrane and regulates Ca^{2+} influx to mitochondria together with mitochondrial calcium uniporter (MCU) (*Hoppe UC, 2010*). Interestingly, IP_3R and VDAC in MAM can not interact directly, but require a linker protein, GRP75 (*Szabadkai G, 2006*).

On the other hand, TS causes ER stress and mitochondrial depolarization. Hence, there is possibility that TS enhances ER mitochondrial contact by regulating or translocating GRP75 to the MAM and increase calcium transfer from ER to the mitochondria. The elevated calcium level in the mitochondria may result in permeability transition pore opening and cytochrome c release leading to apoptosis (*Rutter GA, 2000*). However, the experimental evidence to support this relationship between ER and mitochondria in TS induced apoptosis is unavailable. To investigate, I have examined the effect of TS on ER-mitochondria contact and GRP75 activity.

3.2 Materials and Methods

3.2.1 Materials

TS and egg phosphatidylcholine were purchased from Sigma-Aldrich (St. Louis, MO, USA). D-α-tocopherol were purchased from Tokyo Chemical Industry (Tokyo, Japan). Other reagents were of the highest grade commercially available.

3.2.2 Liposome preparation

A chloroform solution (0.1 mL) containing 0.1 M TS was mixed with 0.64 mL of a chloroform solution containing egg phosphatidylcholine (0.1 g/mL) in a glass tube. The mixture was evaporated to dryness under a nitrogen stream to form a lipid film. The lipid film was hydrated with 192 μL PBS and 8 μL 1 N NaOH. The hydrated lipid film was incubated at 55 °C for 10 min in a water bath. After the incubation, the glass test tube was sonicated in an ultrasonic bath for 10 to 15 minutes to form liposomes. The size and surface charge of the liposomes was measured with a Zetasizer Nano (Malvern Panalytical Ltd., UK).

3.2.3 Cell culture

Mouse melanoma B16F1 cells were purchased from American Type Culture Collection and were cultured in Dulbecco's modified Eagle medium (DMEM) containing 10% fetal bovine serum (FBS) and 1% penicillin-streptomycin at 37 °C in a 5% CO_2 humidified environment. When the cells reached 80% confluency, they were treated with TS or 2-APB for 6 h. In the case of TS+2APB group, 50 μM 2-APB was added 30 minutes prior to TS treatment.

3.2.4 Determination of the ER-mitochondria contact site

After treatment with TS-containing liposomes and 2-APB, cells were washed twice with 0.5 mL PBS. Then, cells were incubated with 500 nM MitoTracker (#8778, Cell Signaling Technology) for 30 min at 37 °C. After that, cells were fixed with 4% paraformaldehyde in PBS for 15 min at 37 °C. Following three washes with PBS containing 1% bovine serum albumin (BSA), cells were permeabilized for 15 min at 37 °C with a PBS solution containing 1% BSA and 0.1% Triton X-100. The cells were washed and incubated with 1 mL culture medium containing 1 μL CytoPainter red detection reagent (ab139482, Abcam) for 30 min at 37 °C. Following several washes with assay buffer of CytoPainter kit, nuclei were counterstained for 15 min with DAPI solution (1 μg/mL). The cells were washed with PBS and

observed with an LSM700 confocal laser scanning microscope. I performed quantitative analysis by drawing the ROI around boundaries of 4-5 cells/image and measuring the area of the yellow signal area by the “color threshold” function of the ImageJ. At least 30 images were analyzed during each observation.

3.2.5 Real-time PCR

Total RNA was extracted and purified from cells with NucleoSpin RNA isolation and purification kit (Takara Bio) according to the manufacturer's instructions. The total RNA concentration was determined with a Nanodrop 8000 spectrometer (Thermo Fisher Scientific). Then, cDNA was synthesized from 200 ng of total RNA with PrimeScript RT Master Mix (Perfect Real Time, Takara Bio, Otsu, Japan) using an MJ Mini Personal Thermal Cycler (Bio-Rad, Hercules, CA, USA). The reverse transcription reaction was performed at 37 °C for 15 min and 85 °C for 5 s. Real-time PCR analysis was performed using TB Green™ Premix Ex Taq™ II (Tli RNaseH Plus, Takara Bio) and a Thermal Cycler Dice Real-Time System III (Takara Bio). To analyze the mRNA levels of GRP75 and GAPDH, the cDNA was denatured at 95 °C for 30 s, followed by 40 cycles of 95 °C for 5 s and 60 °C for 30 s for amplification. The sequences of the primers used for the real-time PCR are shown in Table 2. The mRNA level of GRP78 was calculated using the $2^{-\Delta\Delta Ct}$ method by normalization relative to GAPDH.

Table 2. Sequences of primers used for real-time PCR

Primer	Sequence (5’ to 3’)
Mouse GRP75 forward	GCGTCTTATTGGACGACGAT
Mouse GRP75 reverse	TGGCCCGTAATTTTCTGC
Mouse GAPDH forward	GAGGACCAGGTTGTCTCCTG
Mouse GAPDH reverse	ATGTAGGCCATGAGGTCCAC

3.2.6 Western blotting

The following antibodies were used: anti-GRP75 rabbit monoclonal antibody (Cell Signaling Technology, Danvers, MA, U.S.A), anti-β actin rabbit polyclonal (ab8227, Abcam), and anti-horseradish peroxidase (HRP)-conjugated goat anti-rabbit IgG polyclonal antibody (A24531; Thermo Fisher Scientific, Waltham, MA, USA). To observe the expression of GRP75 in TS and 2-APB treated cells, total protein (10 μg) was separated with 10% SDS-

PAGE, and the proteins were electrophoretically transferred to a polyvinylidene difluoride membrane (Bio-Rad, Hercules, CA, USA). The membrane was incubated with 5% skim milk dissolved in Tris-buffered saline (pH 7.4) containing 0.1% Tween 20 for 1h at 37 °C, then with anti-GRP78 antibody (1:3000) for 24 h at 4 °C. The membrane was washed and incubated with the HRP-conjugated secondary antibody at a dilution of 1:4000 for 1 h at 37 °C. After incubation of the membrane with a chemiluminescent substrate reagent (ECL Prime; GE Healthcare, Little Chalfont, UK), bands were detected with an LAS-4000 mini system (Fuji Film, Tokyo, Japan). After GRP75 was detected, the membrane was washed three times for 45 minutes with Tri-buffered saline (pH 7.4) containing 0.1% Tween 20, incubated with an anti-β actin antibody (1:3000) for 24 h at 4 °C, and developed as above. Band intensities were quantified using ImageJ.

3.2.7 Statistical analysis

Statistical significance was determined using one-way ANOVA to compare multiple groups, followed by Tukey's honestly significant difference test using JASP software. P values less than 0.05 were considered to indicate statistical significance.

3.3 Results

3.3.1 Effect of TS on ER-mitochondria contact site formation

To investigate the effect of TS on ER-mitochondria contact site formation, I treated the mouse melanoma B16F1 cells with TS and IP_3R antagonist, 2-APB. After 6 h of treatment, I stained mitochondria with mitochondria specific dye, MitoTracker (red) and endoplasmic reticulum specific dye cytopainter (green). The yellow fluorescence in the merged images represents the overlapping of mitochondria and ER specific fluorescence and considered as ER-mitochondria contact region. I observed that TS-treated B16F1 cells showed increased yellow fluorescence compared to control, while yellow fluorescence was similar to control cells in 2-APB treated cells (Fig. 3.1A). However, 2-APB treatment reduced yellow fluorescence in TS-treated cells. Upon quantification of the yellow fluorescence by the colour thresholding method of the image analysis, I found TS treated cells exhibited around 167% yellow fluorescence intensity in ER-relative to control (Fig. 3.1B). On the other hand, 2-APB treatment itself did not show any change in yellow fluorescence intensity compared to control. However, the yellow fluorescence intensity was around 102% in cells treated with both 2-APB and TS.

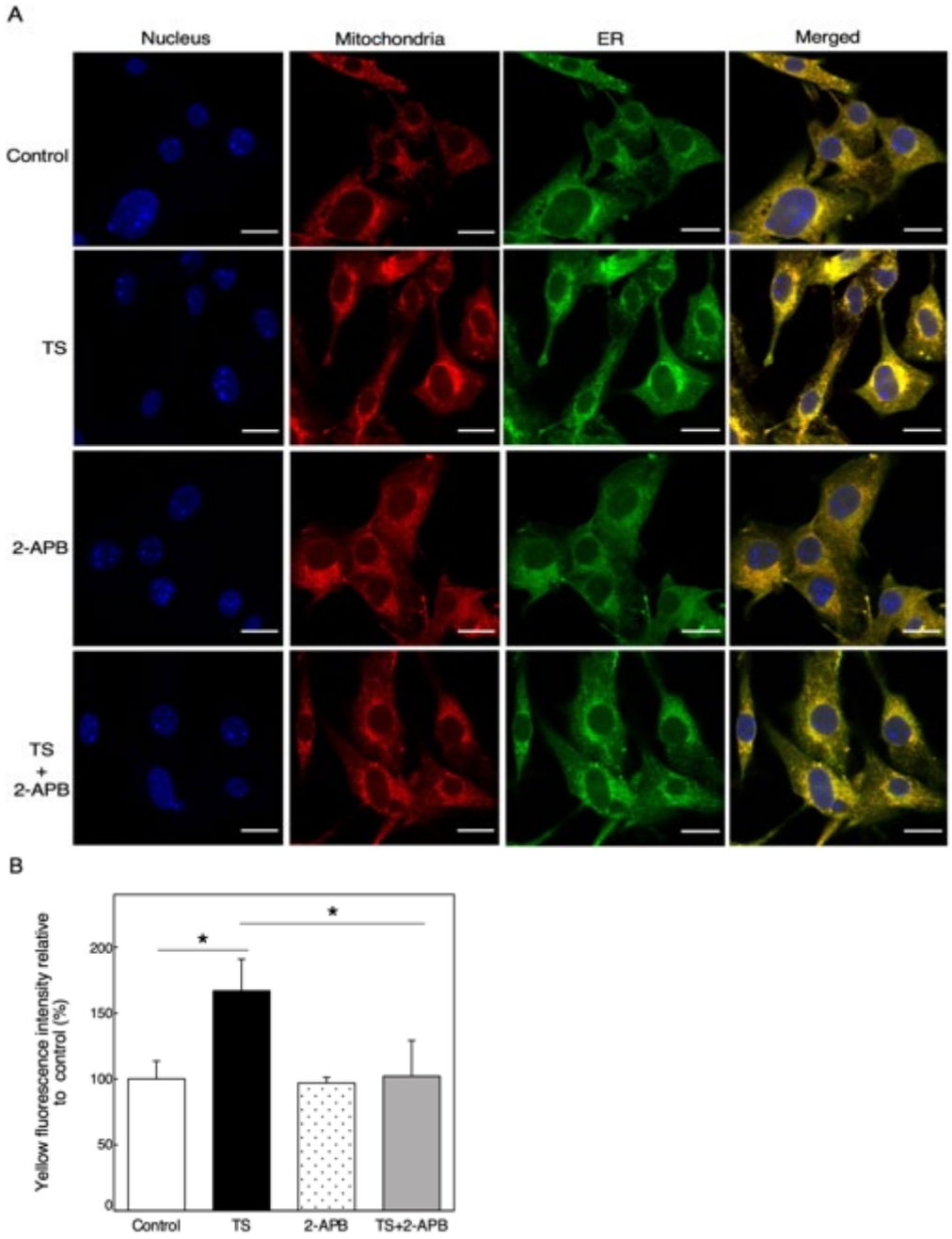

Fig. 3.1 Effects of TS on ER-mitochondria contact site formation

B16F1 cells were separately treated with 75 μM TS containing liposomes and 50 μM 2-APB for 6 h. Cells were incubated in MitoTracker (red) and fixed and permeabilized prior to staining with an ER specific fluorophore cytopainter (green). Nuclei were counterstained with DAPI (blue). (A) Mitochondria (red) and ER (green) were observed after the noted treatments. Yellow fluorescence in the merged images represents ER-mitochondria contact region (B) Percentage of yellow fluorescence intensity. Data are shown as mean ± SD (n = 3). *, $P < 0.05$ (one way ANOVA; Tukey's Post hoc test). Scale bar = 20 μm.

3.3.2 Effect of TS on total GRP75 protein

The IP_3R–GRP75–VDAC complex enhances the ER–mitochondria interaction. Thus the expression of GRP75 may influence the formation of this complex, thereby affecting the ER-mitochondria interaction. Therefore, I examined the GRP78 protein activity in TS- and 2-APB-treated B16F1 cells. To analyze the activity of GRP75 on TS and 2-APB treated mouse melanoma B16F1 cells, I used real-time PCR to quantify the mRNA expressed from the *HSP9A* gene, which encodes for GRP75. The RT-PCR signal from GRP75 mRNA was normalized to that of the housekeeping gene *GAPDH* so as to control for cytotoxic effects. I found that the GRP75 mRNA level is higher in TS-treated B16F1 cells compared to control (Fig. 3.2A). However, the GRP75 mRNA was lower in 2-APB treated cells relative to control and TS-treated cells. The GRP75 mRNA in TS-treated B16F1 cells was around 122% of that of control cells. In contrast, GRP75 mRNA was around 71% relative to control in 2-APB treated cells. In addition, 2-APB treatment reduced GRP75 mRNA level to around 96% that of control. I also assessed GRP75 protein level by western blotting. GRP75 protein level showed an increased tendency in both TS- and 2-APB treated cells (Fig. 3.2B and Fig. 3.2C).

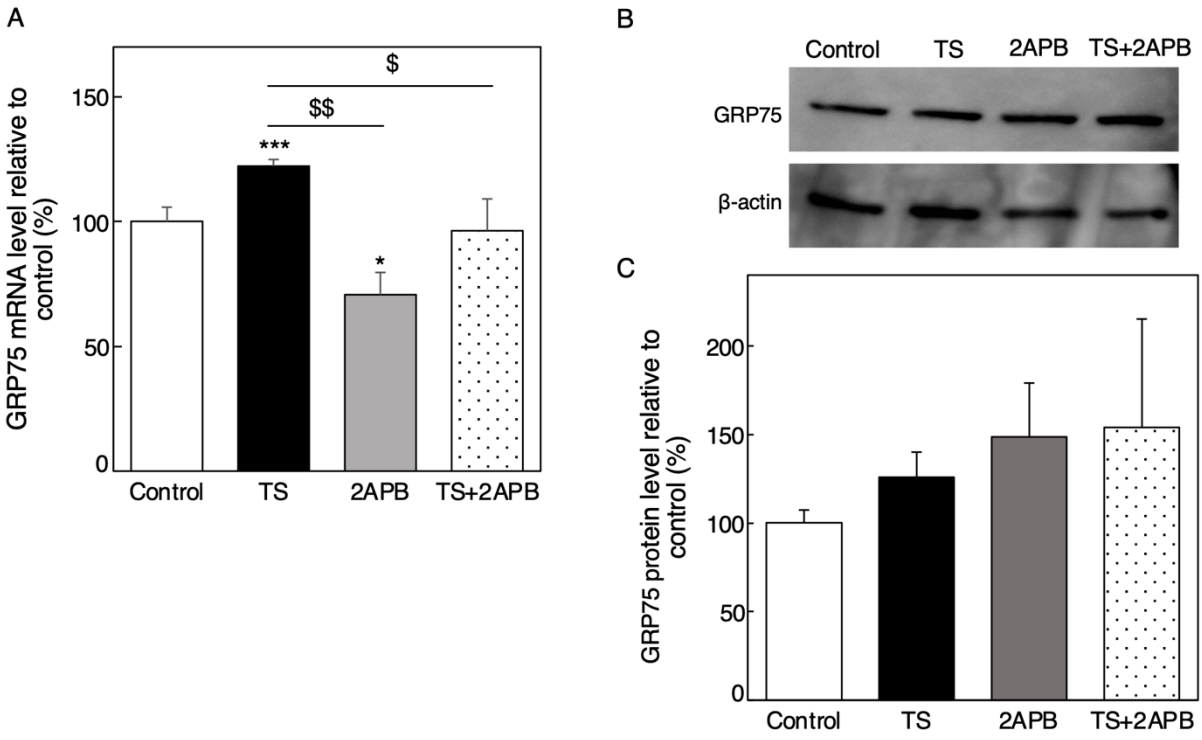

Fig. 3.2 Effect of TS and 2-APB on total GRP75 activity

B16F1 cells were treated with 75 μM TS-containing liposomes and 50 μM 2-APB. Total RNA was isolated after 6 h of treatment, and quantitative real time-PCR was performed (n = 3). Shown are levels of GRP75 mRNA relative to that of the housekeeping gene *GAPDH*. (A) Quantification of GRP75 mRNA in TS and 2-APB treated B16F1 cells. The whole-cell lysate was collected from control cells and cells treated with 75 μM TS-containing liposomes and 50 μM 2-APB and Western blotting was performed, with β-actin serving as an internal control. The intensities of protein bands were quantified by ImageJ. (B) GRP75 protein bands (C) Quantification of GRP75 protein bands. Data are shown as mean ± SD (n = 3). * $P < 0.05$ vs control; *** $P < 0.001$ vs control; $ $P < 0.05$; $$ $P < 0.001$ (one way ANOVA; Tukey's Post hoc test).

3.4 Discussion

In previous reports, it was proposed that TS causes apoptosis by inducing oxidative stress and ER stress. However, the effect of TS on intracellular Ca^{2+} homeostasis which is one of the major regulators of apoptosis not elucidated. In addition, the effect of TS on the MAM which is the major region for Ca^{2+} exchange between ER and mitochondria is unknown. Therefore, to demonstrate how TS regulates Ca^{2+} transfer from ER to mitochondria leading to apoptosis, I studied the effect of TS on MAM. I found that TS treatment increased ER-mitochondria contact in B16F1 cells (Fig. 3.1). However, pretreatment by IP_3R antagonist 2-APB that inhibits Ca^{2+} efflux from ER, diminishes the TS induced increase in ER-mitochondria contact. These findings suggest that Ca^{2+} efflux from ER is essential for ER-mitochondria contact formation. GRP75, a heat shock protein-70 (HSP70) family chaperone that aids ER-mitochondria contact formation by linking up IP_3R and VDAC channel. Thus, GRP75 expression may play critical role in TS induced ER-mitochondria contact formation. I found GRP75 mRNA increased upon TS treatment while 2-APB treatment did not affect GRP75 mRNA level (Fig. 3.2A). However, the western blotting result suggests that GRP75 protein showed an increasing trend in both TS and 2-APB treated cells. These results indicate that, there is no influence of Ca^{2+} efflux from ER on GRP75 protein level. Therefore, the TS-induced upregulation of GRP75 protein may not be responsible for TS-induced ER-mitochondria contact formation. Ca^{2+} plays a key role in signal transduction by binding and changing the conformation of the proteins (*Grzybowska E, 2018*). Moreover, another research group proposed that human HSP70 chaperone family proteins bind with two Ca^{2+} ions within the N-terminal ATPase domain (*Sriram M, 1997*). Taken together, there is possibility that Ca^{2+} released from ER may bind with GRP75 protein and change conformation of GRP75 that aids IP_3R–GRP75–VDAC complex formation. The decrease in ER-mitochondria contact by Ca^{2+} efflux inhibitor 2-APB in TS treated cells supports this hypothesis. However, further investigation is required to fully understand the underlying mechanism of TS induced ER-mitochondria contact site formation.

3.5 Conclusion

TS brings ER and mitochondria closer to each other by enhancing IP_3R–GRP75–VDAC complex formation. Ca^{2+} efflux from ER plays a critical role in this complex formation. The enhanced contact between ER and mitochondria facilitates the flow of Ca^{2+} from ER to mitochondria causing mitochondrial Ca^{2+} overload leading to cellular apoptosis. Hence, I propose that the alteration Ca^{2+} homeostasis in the cancer cells by TS is responsible for TS

induced apoptosis. Nonetheless, IP_3R–GRP75–VDAC complex could be a promising target for the treatment of cancer.

List of Abbreviations

2-APB	2-aminoethyl diphenylborinate
AcOEt	Ethanol ethylacetate
CTCF	Corrected total cell fluorescence
DAPI	4′,6-diamidino-2-phenylindole
ER	Endoplasmic reticulum
GRP75	Glucose regulated protein 75 kDa
GRP78	Glucose regulated protein 78 kDa
HPLC	High performance liquid chromatography
HSP5A	Heat shock protein family A member 5
IP_3	Inositol 1,4,5-triphosphate
IP_3R	Inositol 1,4,5-triphosphate receptor
MAM	Mitochondria associated ER membrane
MCU	Mitochondrial Ca^{2+} uniporter
NAC	N-acetyl cysteine
PKC	Protein kinase C
PQC	Protein quality control
ROI	Region of interest
ROS	Reactive oxygen species
Tglu	α-Tocopheryl glutarate
TMRE	Tetramethyl rhodamine ethyl ester
TS	α-Tocopheryl succinate
UPR	Unfolded protein response
VDAC	Voltage dependent anion channel

Chapter 4

References

Chapter 4: References

Ahumada-Castro, U., Bustos, G., Silva-Pavez, E., Puebla-Huerta, A., Lovy, A., & Cárdenas, C. (2021). In the Right Place at the Right Time: Regulation of Cell Metabolism by IP3R-Mediated Inter-Organelle Ca^{2+} Fluxes. *Frontiers in Cell and Developmental Biology*, *9*. https://doi.org/10.3389/fcell.2021.629522

Aires, V., Hichami, A., Filomenko, R., Plé, A., Rébé, C., Bettaieb, A., & Khan, N. A. (2007). Docosahexaenoic Acid Induces Increases in $[Ca^{2+}]$ via Inositol 1,4,5-Triphosphate Production and Activates Protein Kinase Cγ and -δ via Phosphatidylserine Binding Site: Implication in Apoptosis in U937 Cells. *Molecular Pharmacology*, *72*(6), 1545–1556. https://doi.org/10.1124/mol.107.039792

Azzi, A., Gysin, R., Kempná, P., Ricciarelli, R., Villacorta, L., Visarius, T., & Zingg, J.-M. . (2003). The role of α-tocopherol in preventing disease: from epidemiology to molecular events. *Molecular Aspects of Medicine*, *24*(6), 325–336. https://doi.org/10.1016/s0098-2997(03)00028-1

Berridge, M. J., Lipp, P., & Bootman, M. D. (2000). The versatility and universality of calcium signalling. *Nature Reviews Molecular Cell Biology*, *1*(1), 11–21. https://doi.org/10.1038/35036035

Birringer, M., EyTina, J. H., Salvatore, B. A., & Neuzil, J. (2003). Vitamin E analogues as inducers of apoptosis: structure–function relation. *British Journal of Cancer*, *88*(12), 1948–1955. https://doi.org/10.1038/sj.bjc.6600981

Booth, L., Cazanave, S. C., Hamed, H. A., Yacoub, A., Ogretmen, B., Chen, C.-S., Grant, S., & Dent, P. (2012). OSU-03012 suppresses GRP78/BiP expression that causes PERK-dependent increases in tumor cell killing. *Cancer Biology & Therapy*, *13*(4), 224–236. https://doi.org/10.4161/cbt.13.4.18877

Bukau, B., Weissman, J., & Horwich, A. (2006). Molecular Chaperones and Protein Quality Control. *Cell*, *125*(3), 443–451. https://doi.org/10.1016/j.cell.2006.04.014

Chao, M.-W., Chen, T.-H., Huang, H.-L., Chang, Y.-W., HuangFu, W.-C., Lee, Y.-C., Teng, C.-M., & Pan, S.-L. (2017). Lanatoside C, a cardiac glycoside, acts through protein kinase Cδ to cause apoptosis of human hepatocellular carcinoma cells. *Scientific Reports*, *7*(1). https://doi.org/10.1038/srep46134

Chow CK. (2001). Vitamin E regulation of mitochondrial superoxide generation. *Biol Signals Recept,* 10(1-2):112-24. https://doi.org/10.1159/000046879

Clapham, D. E. (2007). Calcium Signaling. *Cell*, *131*(6), 1047–1058. https://doi.org/10.1016/j.cell.2007.11.028

Csordás, G., Várnai, P., Golenár, T., Roy, S., Purkins, G., Schneider, T. G., Balla, T., & Hajnóczky, G. (2010). Imaging Interorganelle Contacts and Local Calcium Dynamics at the ER-Mitochondrial Interface. *Molecular Cell*, *39*(1), 121–132. https://doi.org/10.1016/j.molcel.2010.06.029

D'Eletto, M., Rossin, F., Occhigrossi, L., Farrace, M. G., Faccenda, D., Desai, R., Marchi, S., Refolo, G., Falasca, L., Antonioli, M., Ciccosanti, F., Fimia, G. M., Pinton, P., Campanella, M., & Piacentini, M. (2018). Transglutaminase Type 2 Regulates ER-Mitochondria Contact Sites by Interacting with GRP75. *Cell Reports*, *25*(13), 3573-3581.e4. https://doi.org/10.1016/j.celrep.2018.11.094

Dauer, P., Sharma, N. S., Gupta, V. K., Durden, B., Hadad, R., Banerjee, S., Dudeja, V., Saluja, A., & Banerjee, S. (2019). ER stress sensor, glucose regulatory protein 78 (GRP78) regulates redox status in pancreatic cancer thereby maintaining "stemness." *Cell Death & Disease*, *10*(2). https://doi.org/10.1038/s41419-019-1408-5

Deniaud, A., Sharaf el dein, O., Maillier, E., Poncet, D., Kroemer, G., Lemaire, C., & Brenner, C. (2007). Endoplasmic reticulum stress induces calcium-dependent permeability transition, mitochondrial outer membrane permeabilization and apoptosis. *Oncogene*, *27*(3), 285–299. https://doi.org/10.1038/sj.onc.1210638

Dong, L-F., Low, P., Dyason, J. C., Wang, X-F., Prochazka, L., Witting, P. K., Freeman, R., Swettenham, E., Valis, K., Liu, J., Zobalova, R., Turanek, J., Spitz, D. R., Domann, F.

E., Scheffler, I. E., Ralph, S. J., & Neuzil, J. (2008). α-Tocopheryl succinate induces apoptosis by targeting ubiquinone-binding sites in mitochondrial respiratory complex II. *Oncogene*, *27*(31), 4324–4335. https://doi.org/10.1038/onc.2008.69

Dos Santos, G. A. S., Abreu e Lima, R. S., Pestana, C. R., Lima, A. S. G., Scheucher, P. S., Thomé, C. H., Gimenes-Teixeira, H. L., Santana-Lemos, B. A. A., Lucena-Araujo, A. R., Rodrigues, F. P., Nasr, R., Uyemura, S. A., Falcão, R. P., de Thé, H., Pandolfi, P. P., Curti, C., & Rego, E. M. (2011). (+)α-Tocopheryl succinate inhibits the mitochondrial respiratory chain complex I and is as effective as arsenic trioxide or ATRA against acute promyelocytic leukemia in vivo. *Leukemia*, *26*(3), 451–460. https://doi.org/10.1038/leu.2011.216

Elfiky, A. A., Baghdady, A. M., Ali, S. A., & Ahmed, M. I. (2020). GRP78 targeting: Hitting two birds with a stone. *Life Sciences*, *260*, 118317. https://doi.org/10.1016/j.lfs.2020.118317

Fasano, E., Serini, S., Piccioni, E., Toesca, A., Monego, G., Cittadini, A. R., Ranelletti, F. O., & Calviello, G. (2012). DHA induces apoptosis by altering the expression and cellular location of GRP78 in colon cancer cell lines. *Biochimica et Biophysica Acta*, *1822*(11), 1762–1772. https://doi.org/10.1016/j.bbadis.2012.08.003

Feng, K., Ge, Y., Chen, Z., Li, X., Liu, Z., Li, X., Li, H., Tang, T., Yang, F., & Wang, X. (2019). Curcumin Inhibits the PERK-eIF2α-CHOP Pathway through Promoting SIRT1 Expression in Oxidative Stress-induced Rat Chondrocytes and Ameliorates Osteoarthritis Progression in a Rat Model. *Oxidative Medicine and Cellular Longevity*, *2019*, 1–17. https://doi.org/10.1155/2019/8574386

Folch, J., Lees, M., & Stanley, G. H. S. (1957). A Simple Method for the Isolation and Purification of Total Lipids from Animal Tissues. *Journal of Biological Chemistry*, *226*(1), 497–509. https://doi.org/10.1016/s0021-9258(18)64849-5

Fu, X., Cui, J., Meng, X., Jiang, P., Zheng, Q., Zhao, W., & Chen, X. (2021). Endoplasmic reticulum stress, cell death and tumor: Association between endoplasmic reticulum

stress and the apoptosis pathway in tumors (Review). *Oncology Reports*, *45*(3), 801–808. https://doi.org/10.3892/or.2021.7933

Galluzzi, L., Bravo-San Pedro, J. M., & Kroemer, G. (2014). Organelle-specific initiation of cell death. *Nature Cell Biology*, *16*(8), 728–736. https://doi.org/10.1038/ncb3005

Giacomello, M., & Pellegrini, L. (2016). The coming of age of the mitochondria–ER contact: a matter of thickness. *Cell Death & Differentiation*, *23*(9), 1417–1427. https://doi.org/10.1038/cdd.2016.52

Giamogante, F., Poggio, E., Barazzuol, L., Covallero, A., & Calì, T. (2021). Apoptotic signals at the endoplasmic reticulum-mitochondria interface. *Apoptosis in Health and Disease - Part B*, 307–343. https://doi.org/10.1016/bs.apcsb.2021.02.007

Giorgi, C., Baldassari, F., Bononi, A., Bonora, M., De Marchi, E., Marchi, S., Missiroli, S., Patergnani, S., Rimessi, A., Suski, J. M., Wieckowski, M. R., & Pinton, P. (2012). Mitochondrial Ca^{2+} and apoptosis. *Cell Calcium*, *52*(1), 36–43. https://doi.org/10.1016/j.ceca.2012.02.008

Görlach, A., Bertram, K., Hudecova, S., & Krizanova, O. (2015). Calcium and ROS: A mutual interplay. *Redox Biology*, *6*, 260–271. https://doi.org/10.1016/j.redox.2015.08.010

Grzybowska, E. (2018). Calcium-Binding Proteins with Disordered Structure and Their Role in Secretion, Storage, and Cellular Signaling. *Biomolecules*, *8*(2), 42. https://doi.org/10.3390/biom8020042

Ha, D. P., Tsai, Y.-L., & Lee, A. S. (2021). Suppression of ER-stress induction of GRP78 as an anti-neoplastic mechanism of the cardiac glycoside Lanatoside C in pancreatic cancer: Lanatoside C suppresses GRP78 stress induction. *Neoplasia*, *23*(12), 1213–1226. https://doi.org/10.1016/j.neo.2021.10.004

Hamasaki, M., Furuta, N., Matsuda, A., Nezu, A., Yamamoto, A., Fujita, N., Oomori, H., Noda, T., Haraguchi, T., Hiraoka, Y., Amano, A., & Yoshimori, T. (2013). Autophagosomes

form at ER–mitochondria contact sites. *Nature*, *495*(7441), 389–393. https://doi.org/10.1038/nature11910

Hoppe, U. C. (2010). Mitochondrial calcium channels. *FEBS Letters*, *584*(10), 1975–1981. https://doi.org/10.1016/j.febslet.2010.04.017

Hsu, S.-K., Chiu, C.-C., Dahms, H.-U., Chou, C.-K., Cheng, C.-M., Chang, W.-T., Cheng, K.-C., Wang, H.-M. D., & Lin, I-Ling. (2019). Unfolded Protein Response (UPR) in Survival, Dormancy, Immunosuppression, Metastasis, and Treatments of Cancer Cells. *International Journal of Molecular Sciences*, *20*(10). https://doi.org/10.3390/ijms20102518

Huang, X., Li, L., Zhang, L., Zhang, Z., Wang, X., Zhang, X., Hou, L., & Wu, K. (2012). Crosstalk between endoplasmic reticulum stress and oxidative stress in apoptosis induced by α-tocopheryl succinate in human gastric carcinoma cells. *British Journal of Nutrition*, *109*(4), 727–735. https://doi.org/10.1017/s0007114512001882

Huang, X., Zhang, Z., Jia, L., Zhao, Y., Zhang, X., & Wu, K. (2010). Endoplasmic reticulum stress contributes to vitamin E succinate-induced apoptosis in human gastric cancer SGC-7901 cells. *Cancer Letters*, *296*(1), 123–131. https://doi.org/10.1016/j.canlet.2010.04.002

Ibrahim, I. M., Abdelmalek, D. H., & Elfiky, A. A. (2019). GRP78: A cell's response to stress. *Life Sciences*, *226*, 156–163. https://doi.org/10.1016/j.lfs.2019.04.022

Joseph, S. K., & Hajnóczky, G. (2007). IP3 receptors in cell survival and apoptosis: Ca^{2+} release and beyond. *Apoptosis*, *12*(5), 951–968. https://doi.org/10.1007/s10495-007-0719-7

Kang, Y.-H., Lee, E., Choi, M.-K., Ku, J.-L., Kim, S. H., Park, Y.-G., & Lim, S.-J. (2004). Role of reactive oxygen species in the induction of apoptosis by α-tocopheryl succinate. *International Journal of Cancer*, *112*(3), 385–392. https://doi.org/10.1002/ijc.20424

Kania, E., Roest, G., Vervliet, T., Parys, J. B., & Bultynck, G. (2017). IP3 Receptor-Mediated Calcium Signaling and Its Role in Autophagy in Cancer. *Frontiers in Oncology*, *7*. https://doi.org/10.3389/fonc.2017.00140

Kao, C., Chandna, R., Ghode, A., Dsouza, C., Chen, M., Larsson, A., Lim, S. H., Wang, M., Cao, Z., Zhu, Y., Anand, G. S., & Ge, R. (2018). Proapoptotic Cyclic Peptide BC71 Targets Cell-Surface GRP78 and Functions as an Anticancer Therapeutic in Mice. *EBioMedicine*, *33*, 22–32. https://doi.org/10.1016/j.ebiom.2018.06.004

Kara, M., & Oztas, E. (2020). Endoplasmic Reticulum Stress-Mediated Cell Death. *Programmed Cell Death*. https://doi.org/10.5772/intechopen.85401

Kluckova, K., Bezawork-Geleta, A., Rohlena, J., Dong, L., & Neuzil, J. (2013). Mitochondrial complex II, a novel target for anti-cancer agents. *Biochimica et Biophysica Acta (BBA) - Bioenergetics*, *1827*(5), 552–564. https://doi.org/10.1016/j.bbabio.2012.10.015

Kogure, K., Hama, S., Kisaki, M., Takemasa, H., Tokumura, A., Suzuki, I., & Fukuzawa, K. (2004). Structural characteristic of terminal dicarboxylic moiety required for apoptogenic activity of α-tocopheryl esters. *Biochimica et Biophysica Acta (BBA) - General Subjects*, *1672*(2), 93–99. https://doi.org/10.1016/j.bbagen.2004.03.001

Kogure, K., Hama, S., Manabe, S., Tokumura, A., & Fukuzawa, K. (2002). High cytotoxicity of α-tocopheryl hemisuccinate to cancer cells is due to failure of their antioxidative defense systems. *Cancer Letters*, *186*(2), 151–156. https://doi.org/10.1016/s0304-3835(02)00344-0

Kogure, K., Manabe, S., Suzuki, I., Tokumura, A., & Fukuzawa, K. (2005). Cytotoxicity of α-Tocopheryl Succinate, Malonate and Oxalate in Normal and Cancer Cells In Vitro and Their Anti-Cancer Effects on Mouse Melanoma In Vivo. *Journal of Nutritional Science and Vitaminology*, *51*(6), 392–397. https://doi.org/10.3177/jnsv.51.392

Kogure, K., Morita, M., Nakashima, S., Hama, S., Tokumura, A., & Fukuzawa, K. (2001). Superoxide is responsible for apoptosis in rat vascular smooth muscle cells induced by

α-tocopheryl hemisuccinate. *Biochimica et Biophysica Acta (BBA) - General Subjects*, *1528*(1), 25–30. https://doi.org/10.1016/s0304-4165(01)00168-4

Koong, A. C., Auger, E. A., Chen, E. Y., & Giaccia, A. J. (1994). The Regulation of GRP78 and Messenger RNA Levels by Hypoxia Is Modulated by Protein Kinase C Activators and Inhibitors. *Radiation Research*, *138*(1), S60. https://doi.org/10.2307/3578763

Krebs, J., Agellon, L. B., & Michalak, M. (2015). Ca^{2+} homeostasis and endoplasmic reticulum (ER) stress: An integrated view of calcium signaling. *Biochemical and Biophysical Research Communications*, *460*(1), 114–121. https://doi.org/10.1016/j.bbrc.2015.02.004

Lebeau, P. F., Platko, K., Byun, J. H., & Austin, R. C. (2021). Calcium as a reliable marker for the quantitative assessment of endoplasmic reticulum stress in live cells. *Journal of Biological Chemistry*, *296*, 100779. https://doi.org/10.1016/j.jbc.2021.100779

Leiva-Rodríguez, T., Romeo-Guitart, D., Herrando-Grabulosa, M., Muñoz-Guardiola, P., Polo, M., Bañuls, C., Petegnief, V., Bosch, A., Lizcano, J. M., Apostolova, N., Forés, J., & Casas, C. (2021). GRP78 Overexpression Triggers PINK1-IP3R-Mediated Neuroprotective Mitophagy. *Biomedicines*, *9*(8), 1039. https://doi.org/10.3390/biomedicines9081039

Lewis, S. C., Uchiyama, L. F., & Nunnari, J. (2016). ER-mitochondria contacts couple mtDNA synthesis with mitochondrial division in human cells. *Science (New York, N.Y.)*, *353*(6296), aaf5549. https://doi.org/10.1126/science.aaf5549

Li, J., Qi, F., Su, H., Zhang, C., Zhang, Q., Chen, Y., Chen, P., Su, L., Chen, Y., Yang, Y., Chen, Z., & Zhang, S. (2022). GRP75-faciliated Mitochondria-associated ER Membrane (MAM) Integrity controls Cisplatin-resistance in Ovarian Cancer Patients. *International Journal of Biological Sciences*, *18*(7), 2914–2931. https://doi.org/10.7150/ijbs.71571

Li, Y., Li, H.-Y., Shao, J., Zhu, L., Xie, T.-H., Cai, J., Wang, W., Cai, M.-X., Wang, Z.-L., Yao, Y., & Wei, T.-T. (2022). GRP75 modulates endoplasmic reticulum-mitochondria

coupling and accelerates Ca^{2+}-dependent endothelial cells apoptosis in diabetic retinopathy. *Research Square*. https://doi.org/10.21203/rs.3.rs-2093332/v1

Liang, G., Fang, X., Yang, Y., & Song, Y. (2018). Knockdown of CEMIP suppresses proliferation and induces apoptosis in colorectal cancer cells: downregulation of GRP78 and attenuation of unfolded protein response. *Biochemistry and Cell Biology*, *96*(3), 332–341. https://doi.org/10.1139/bcb-2017-0151

Mahmmoud, Y. A. (2007). Modulation of protein kinase C by curcumin; inhibition and activation switched by calcium ions. *British Journal of Pharmacology*, *150*(2), 200–208. https://doi.org/10.1038/sj.bjp.0706970

Marchi, S., Patergnani, S., & Pinton, P. (2014). The endoplasmic reticulum–mitochondria connection: One touch, multiple functions. *Biochimica et Biophysica Acta (BBA) - Bioenergetics*, *1837*(4), 461–469. https://doi.org/10.1016/j.bbabio.2013.10.015

Martinvalet, D. (2018). The role of the mitochondria and the endoplasmic reticulum contact sites in the development of the immune responses. *Cell Death & Disease*, *9*(3). https://doi.org/10.1038/s41419-017-0237-7

Martucciello, S., Paolella, G., Muzashvili, T., Skhirtladze, A., Pizza, C., Caputo, I., & Piacente, S. (2018). Steroids from Helleborus caucasicus reduce cancer cell viability inducing apoptosis and GRP78 down-regulation. *Chemico-Biological Interactions*, *279*, 43–50. https://doi.org/10.1016/j.cbi.2017.11.002

Martínez Banaclocha M. (2000). N-acetylcysteine elicited increase in complex I activity in synaptic mitochondria from aged mice: implications for treatment of Parkinson's disease. *Brain Res.* 859(1), 173-175. https://doi.org/10.1016/s0006-8993(00)02005-9

Neuzil, J., Wang, X.-F., Dong, L.-F., Low, P., & Ralph, S. J. (2006). Molecular mechanism of "mitocan"-induced apoptosis in cancer cells epitomizes the multiple roles of reactive oxygen species and Bcl-2 family proteins. *FEBS Letters*, *580*(22), 5125–5129. https://doi.org/10.1016/j.febslet.2006.05.072

Neuzil, J., Weber, T., Gellert, N., & Weber, C. (2001). Selective cancer cell killing by α-tocopheryl succinate. *British Journal of Cancer*, *84*(1), 87–89. https://doi.org/10.1054/bjoc.2000.1559

Nowicka, U., Chroscicki, P., Stroobants, K., Sladowska, M., Turek, M., Uszczynska-Ratajczak, B., Kundra, R., Goral, T., Perni, M., Dobson, C. M., Vendruscolo, M., & Chacinska, A. (2021). Cytosolic aggregation of mitochondrial proteins disrupts cellular homeostasis by stimulating the aggregation of other proteins. *ELife*, *10*. https://doi.org/10.7554/elife.65484

Ojha, R., & Amaravadi, R. K. (2017). Targeting the unfolded protein response in cancer. *Pharmacological Research*, *120*, 258–266. https://doi.org/10.1016/j.phrs.2017.04.003

Ott, M., Robertson, J. D., Gogvadze, V., Zhivotovsky, B., & Orrenius, S. (2002). Cytochrome c release from mitochondria proceeds by a two-step process. *Proceedings of the National Academy of Sciences*, *99*(3), 1259–1263. https://doi.org/10.1073/pnas.241655498

Ouyang, Y.-B., Xu, L.-J., Emery, J. F., Lee, A. S., & Giffard, R. G. (2011). Overexpressing GRP78 influences Ca^{2+} handling and function of mitochondria in astrocytes after ischemia-like stress. *Mitochondrion*, *11*(2), 279–286. https://doi.org/10.1016/j.mito.2010.10.007

Papas, A. M. (1993). Oil-Soluble Antioxidants in Foods. *Toxicology and Industrial Health*, *9*(1-2), 123–149. https://doi.org/10.1177/0748233793009001-210

Prasad, K. N., Kumar, B., Yan, X.-D., Hanson, A. J., & Cole, W. C. (2003). α-Tocopheryl Succinate, the Most Effective Form of Vitamin E for Adjuvant Cancer Treatment: A Review. *Journal of the American College of Nutrition*, *22*(2), 108–117. https://doi.org/10.1080/07315724.2003.10719283

Prasad, M., Pawlak, K. J., Burak, W. E., Perry, E. E., Marshall, B., Whittal, R. M., & Bose, H. S. (2017). Mitochondrial metabolic regulation by GRP78. *Science Advances*, *3*(2). https://doi.org/10.1126/sciadv.1602038

Prins, D., & Michalak, M. (2011). Organellar Calcium Buffers. *Cold Spring Harbor Perspectives in Biology*, *3*(3), a004069–a004069. https://doi.org/10.1101/cshperspect.a004069

Rauchová, H., Vokurková, M., & Drahota, Z. (2014). Inhibition of mitochondrial glycerol-3-phosphate dehydrogenase by α-tocopheryl succinate. *The International Journal of Biochemistry & Cell Biology*, *53*, 409–413. https://doi.org/10.1016/j.biocel.2014.06.010

Rieusset, J. (2018). The role of endoplasmic reticulum-mitochondria contact sites in the control of glucose homeostasis: an update. *Cell Death & Disease*, *9*(3). https://doi.org/10.1038/s41419-018-0416-1

Rutter, G. A., & Rizzuto, R. (2000). Regulation of mitochondrial metabolism by ER Ca^{2+} release: an intimate connection. *Trends in Biochemical Sciences*, *25*(5), 215–221. https://doi.org/10.1016/s0968-0004(00)01585-1

Sano, R., & Reed, J. C. (2013). ER stress-induced cell death mechanisms. *Biochimica Et Biophysica Acta (BBA) - Molecular Cell Research*, *1833*(12), 3460–3470. https://doi.org/10.1016/j.bbamcr.2013.06.028

Sharma, S. H., Rajamanickam, V., & Nagarajan, S. (2018). Antiproliferative effect of p-Coumaric acid targets UPR activation by downregulating Grp78 in colon cancer. *Chemico-Biological Interactions*, *291*, 16–28. https://doi.org/10.1016/j.cbi.2018.06.001

Shen, L., Wen, N., Xia, M., Zhang, Y., Liu, W., Xu, Y., & Sun, L. (2016). Calcium efflux from the endoplasmic reticulum regulates cisplatin-induced apoptosis in human cervical cancer HeLa cells. *Oncology Letters*, *11*(4), 2411–2419. https://doi.org/10.3892/ol.2016.4278

Sies, H., & Murphy, M. E. (1991). Role of tocopherols in the protection of biological systems against oxidative damage. *Journal of Photochemistry and Photobiology B: Biology*, *8*(2), 211. https://doi.org/10.1016/1011-1344(91)80061-l

Sriram, M., Osipiuk, J., Freeman, B., Morimoto, R., & Joachimiak, A. (1997). Human Hsp70 molecular chaperone binds two calcium ions within the ATPase domain. *Structure*, *5*(3), 403–414. https://doi.org/10.1016/s0969-2126(97)00197-4

Sugawara, S., Takeda, K., Lee, A. S., & Dennert, G. (1993). Suppression of stress protein GRP78 induction in tumor B/C10ME eliminates resistance to cell mediated cytotoxicity. *Cancer Research*, *53*(24), 6001–6005.

Sun, F.-C., Wei, S., Li, C.-W., Chang, Y.-S., Chao, C.-C., & Lai, Y.-K. (2006). Localization of GRP78 to mitochondria under the unfolded protein response. *Biochemical Journal*, *396*(1), 31–39. https://doi.org/10.1042/bj20051916

Suzuki, Y. J., & Ford, G. D. (1992). Superoxide stimulates IP3-induced Ca^{2+} release from vascular smooth muscle sarcoplasmic reticulum. *American Journal of Physiology-Heart and Circulatory Physiology*, *262*(1), H114–H116. https://doi.org/10.1152/ajpheart.1992.262.1.h114

Szabadkai, G., Bianchi, K., Várnai, P., De Stefani, D., Wieckowski, M. R., Cavagna, D., NagyA. I., BallaT., & Rizzuto, R. (2006). Chaperone-mediated coupling of endoplasmic reticulum and mitochondrial Ca^{2+} channels. *Journal of Cell Biology*, *175*(6), 901–911. https://doi.org/10.1083/jcb.200608073

Szegezdi, E., Logue, S. E., Gorman, A. M., & Samali, A. (2006). Mediators of endoplasmic reticulum stress-induced apoptosis. *EMBO Reports*, *7*(9), 880–885. https://doi.org/10.1038/sj.embor.7400779

Tameire, F., Verginadis, I. I., & Koumenis, C. (2015). Cell intrinsic and extrinsic activators of the unfolded protein response in cancer: Mechanisms and targets for therapy. *Seminars in Cancer Biology*, *33*, 3–15. https://doi.org/10.1016/j.semcancer.2015.04.002

Tiwary, S., Nandwani, A., Khan, R., & Datta, M. (2021). GRP75 mediates endoplasmic reticulum–mitochondria coupling during palmitate-induced pancreatic β-cell apoptosis. *Journal of Biological Chemistry*, *297*(6), 101368. https://doi.org/10.1016/j.jbc.2021.101368

Wadhwa, R., Taira, K., & Kaul, S. C. (2002). An Hsp70 family chaperone, mortalin/mthsp70/PBP74/Grp75: what, when, and where? *Cell Stress & Chaperones*, *7*(3), 309. https://doi.org/10.1379/1466-1268(2002)007<0309:ahfcmm>2.0.co;2

Wu, Y., Zhang, H., Dong, Y., Park, Y.-M., & Ip, C. (2005). Endoplasmic Reticulum Stress Signal Mediators Are Targets of Selenium Action. *Cancer Research*, *65*(19), 9073–9079. https://doi.org/10.1158/0008-5472.can-05-2016

Yan, B., Stantic, M., Zobalova, R., Bezawork-Geleta, A., Stapelberg, M., Stursa, J., Prokopova, K., Dong, L., & Neuzil, J. (2015). Mitochondrially targeted vitamin E succinate efficiently kills breast tumour-initiating cells in a complex II-dependent manner. *BMC Cancer*, *15*(1). https://doi.org/10.1186/s12885-015-1394-7

Yu, X., Shi, L., Yan, L., Wang, H., Wen, Y., & Zhang, X. (2018). Downregulation of glucose-regulated protein 78 enhances the cytotoxic effects of curcumin on human nasopharyngeal carcinoma cells. *International Journal of Molecular Medicine*. https://doi.org/10.3892/ijmm.2018.3837

Yun, S., Han, Y.-S., Lee, J. H., Kim, S., & Lee, S. H. (2017). Enhanced Susceptibility to 5-Fluorouracil in Human Colon Cancer Cells by Silencing of GRP78. *Anticancer Research*, *37*(6). https://doi.org/10.21873/anticanres.11651

Zhao, Q., Luo, T., Gao, F., Fu, Y., Li, B., Shao, X., Chen, H., Zhou, Z., Guo, S., Shen, L., Jin, L., Cen, D., Zhou, H., Lyu, J., & Fang, H. (2021). GRP75 Regulates Mitochondrial-Super complex Turnover to Modulate Insulin Sensitivity. *Diabetes*, *71*(2), 233–248. https://doi.org/10.2337/db21-0173

Acknowledgement

First and foremost, praises and thanks to Allah, the almighty, for His showers of blessings throughout my research to complete the research successfully. It is my pleasure to express my gratitude and appreciate the following individuals who made valuable contributions to complete this thesis work.

I take the opportunity to express my deepest gratitude and sincere, wholehearted appreciation to my honourable supervisor Dr. Kentaro Kogure (Professor, Faculty of Pharmaceutical Sciences, Tokushima University, Japan), for the continuous support to my Ph.D. study and research, for his patience, motivation, enthusiasm, and immense knowledge. He has taught me the methodology to carry out the study, interpretation of the experiment results, scientific manuscript writing and to present the research works as clearly as possible. His guidance and training helped me to grow and think like an independent researcher. I could not have imagined having a better supervisor and mentor for my Ph.D. study.

My heartfelt gratitude to Dr. Mizune Ozono (Assistant Professor, Faculty of Pharmaceutical Sciences, Tokushima University, Japan) for her active supervision, valuable suggestion, and kind co-operation to continue my research work smoothly.

I am indebted to Dr. Shigeki Sano (Professor, Faculty of Pharmaceutical Sciences, Tokushima University, Japan) for his encouragement and all kinds of assistance during my research in Tokushima University.

I express my sincere gratitude to Dr. Michiyasu Nakao (Assistant Professor, Faculty of Pharmaceutical Sciences, Tokushima University, Japan) for his continuous and valuable assistance during my research.

I am very much grateful of Dr. Tatsuya Fukuta (Former Assistant professor, Faculty of Pharmaceutical Sciences) for his heartiest co-operation and valuable suggestions regarding my research.

I would like to utter my sincere thanks to Professor Koichiro Tsuchiya and Professor Tamotsu Tanaka for their valuable support and suggestions to ensure smooth continuation of my study.

I have the pleasure to express my loving thanks to all my fellow labmates for their flawless support and offering me a pleasant research environment.

Last but not least, I am extremely grateful to my family for their love, prayers, caring, and sacrifices.